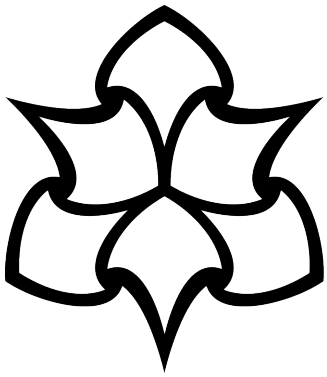

Molybdenum Disulphide Surfaces to Reduce *Staphylococcus aureus* and *Pseudomonas aeruginosa* Biofilm Formation

Mohsin Amin[1], Samuel Rowley-Neale[2], Liliana Shalamanova[1], Stephen Lynch[3], Joels T. Wilson-Nieuwenhuis[1], Mohamed El Mohtadi[1], Craig E. Banks[2] and Kathryn A. Whitehead[1*]

[1]Microbiology at Interfaces, Manchester Metropolitan University, Manchester, UK.

[2]Faculty of Science and Engineering, Manchester Metropolitan University, Manchester, UK.

[3]Department of Computing and Mathematics, Manchester Metropolitan University, Manchester, UK.

ORCID: Mohsin Amin 0000-0003-3873-8820, Samuel Rowley-Neale , Liliana Shalamanova 0000-0003-4606-2234, Stephen Lynch 0000-0002-4183-5122, Joels T. Wilson-Nieuwenhuis 0000-0002-8906-4304, Mohamed El Mohtadi 0000-0002-5707-6415, Craig E. Banks 0000-0002-0756-9764 and Kathryn A. Whitehead 0000-0001-6001-6686

ABSTRACT: The reduction of bacteria and biofilm formation is important when designing surfaces for use in industry. Molybdenum disulphide surfaces (MoS_{2SUR}) were produced using MoS_2 particle (MoS_{2PAR}) sizes of 90 nm 2 µm and 6 µm containing MoS_{2PAR} concentrations of 5%, 10%, 15% and 20%. These were tested to determine the efficacy of the MoS_{2SUR} to impede bacterial retention and biofilm formation of two different types of bacteria, *Staphylococcus aureus* and *Pseudomonas aeruginosa*. The MoS_{2SUR} were characterised using Fourier Transform InfraRed Spectroscopy, Ion Coupled Plasma Atomic Emission Spectroscopy, Scanning Electron Microscopy, Optical Profilometry and Water Contact Angles. The MoS_{2SUR} made with the smaller 90 nm MoS_{2PAR} sizes demonstrated smaller topographical shaped features. As the size of the incorporated MoS_{2PAR} increased, the MoS_{2SUR} demonstrated wider surface features, and they were less wettable. The increase in MoS_{2PAR} concentration within the MoS_{2SUR} groups did not affect the surface topography but did increase wettability. However, the increase in MoS_{2PAR} size increased both the surface topography and wettability. The MoS_{2SUR} with the smaller topographical shaped features, influenced the retention of the *S. aureus* bacteria. Increased MoS_{2SUR} topography and wettability resulted in the greatest reduction in bacterial retention and the bacteria became more heterogeneously dispersed and less clustered across the surfaces. The surfaces that exhibited decreased bacterial retention (largest particle sizes, largest features, greatest roughness, most wettable) resulted in decreased biofilm formation. Cytotoxicity testing of the surface using cell viability demonstrated that the MoS_{2SUR} were not toxic against HK-2 cells at MoS_{2PAR} sizes of 90 nm and 2 µm. This work demonstrated that individual surfaces variables (MoS_{2SUR} topographic shape and roughness, MoS_{2PAR} size and concentration) decreased bacterial loading on the surfaces, which then decreased biofilm formation. By optimising MoS_{2SUR} properties, it was possible to impede bacterial retention and subsequent biofilm formation.

KEYWORDS: *Molybdenum disulphide surfaces*, *Bacteria*, *Biofilms*, *Retention*, *Antifouling*, *Cytotoxicity*

INTRODUCTION

Biofouling is an issue that is of great concern to many industries including the healthcare sector, water and food industries. In the food industry, microbial contamination of surfaces can result in product spoilage, and ultimately lead to health issues of the consumer.[1] Thus, the preference of bacteria to become retained onto a surface is highly undesirable due to the ever present possibility of biotransfer.[2]

The retention of bacterial cells to materials is an initial step in which contamination of surfaces, food products or medical equipment can occur.[3] Bacterial cells typically attach to a surface following a two-step process. Initial, reversible attachment, is thought to influenced more by physicochemical forces while irreversible retention may be more influenced by surface roughness.[4] Planktonic bacteria prefer to be attached to a surface, and once they have attached they form a biofilm.[5] The aggregation of biofilms on abiotic or biotic surfaces are a ubiquitous behaviour of bacteria. The biofilms which bacteria produce are covered by a hydrophilic, exopolymeric substance, which protects the bacteria making them more resilient to antimicrobials.[6] Thus, bacteria in such formations are much more difficult to treat and kill than planktonic bacterial species. This makes biofilm formation a much more difficult problem to treat and/or eradicate. The formation of biofilms in the food processing industries is a leading cause of foodborne disease spread.[7] In clinical settings, the continual presence of biofilms increases the risk of healthcare associated infections (HCAI).[8] Biofilm formation of medical instrumentation or via transmission from water systems may lead to potential pathogen transfer and subsequent increased morbidity and mortality, posing a significant impact on public health and wellbeing.[9] Moreover, the cleaning of surfaces is a substantial financial burden on both the industrial and medical professions.[10]

Key strategies for disrupting bacterial retention may be targeted towards the development of novel surfaces. Although some 2D-materials containing metals have been suggested (reduced graphene oxide/silver in nanocomposite and zinc-graphite composite coatings) there is also a growing requirement for surfaces to be more ecological friendly, and potentially less cytotoxic by using materials that do not leach their individual components.[11,12] Two dimensional (2D) materials and particles have been suggested to demonstrate antifouling activity with low toxicity.[5,13,14] Although much work has been carried out on the antifouling properties of graphite and graphene/graphene oxide amongst nanomaterials, the transition metal dichalcogenides have received little attention in the determination of their ability to impede bacterial retention and subsequent biofilm formation, with minimal cytotoxic properties.[11,15-18] One such material with the potential to be used as a low fouling surface is

MoS_{2SUR}. Molybdenum disulphide is mainly obtained as a secondary product from the mining of copper.[18] Since both molybdenum and sulphur are earth abundant elements, this combined with there being several commercial scale methodologies for producing MoS_2, allow it to be a relatively cheaply sourced material. MoS_{2SUR} potentially has inherent antifouling properties, better than those of other materials such as graphene oxide due to its surface properties. MoS_{2SUR} and MoS_{2PAR} are composed of a monolayer of molybdenum atoms that are between parallel sulphur atom layers which are held together loosely by van der Waals forces.[19,20] MoS_{2SUR} has unique physicochemical and mechanical properties, with a lowered amount of functional groups.[21,22] MoS_{2SUR} also have extremely low friction coefficients which means that fouling it likely to be lowered on such substrates.[23] Thus, the use of such surfaces as antifouling materials may result due to their surface and anti-frictional properties. Investigation into the antifouling nature of such modified surfaces is required, since factors such as surface topography, chemistry and physicochemistry have been demonstrated to influence microbial retention, with microbial retention and subsequent biofilm formation.

Often the relationship between the surface properties and the retention and distribution of bacteria across surfaces is determined using factors such as percentage coverage.[24] However, in order to understand such interactions in more detail, mathematical analysis, such as using multifractal analysis can be used to give further insight into the surface interface:bacterial relationships.[24-26] The relationship between initial bacterial load and the rate of biofilm formation is also unclear. Studies investigating the effects antifouling effects of 2D materials including MoS_{2SUR} are weighted heavily towards testing against planktonic bacteria. However, it is also important to determine the effects that such surfaces have towards bacterial biofilms, since biofilm formations are more prevalent on surfaces in industry and the environment and they are extremely difficult to impede.

The aim of this work was to determine the effect of MoS_{2SUR} on the retention and subsequent biofilm formation of *Staphylococcus aureus* and *Pseudomonas aeruginosa* and determine the cytotoxic effect of the MoS_{2SUR}.

MATERIALS AND METHODS

MoS_{2SUR} Surface Screen Printing. The MoS_{2PAR} were analytical grade and were used as received from Sigma-Aldrich (UK) without further purification. The average lateral width, purity of 98-99%, and a molybdenum content of 58.4% - 61.4% of the MoS_{2PAR} in powder was determined according to the manufacturer specifications (Sigma-Aldrich, UK).[27] To produce MoS_{2PAR} containing surfaces, MoS_{2PAR} sizes of 90 nm, 2 μm and 6 μm (Sigma-Aldrich, UK)

were incorporated into commercially available graphite ink (Gwent Electronic Materials, UK) using the weight percent of MoS_{2PAR} within the mass of the ink formulation used in the printing process;

$$\% = (M_P / M_I) \times 100 \qquad [1]$$

where M_P is the mass of the particulate added and M_I is the total combined weight of the ink formulation. The MoS_{2PAR} containing ink was screen-printed onto an underlying layer of a cured carbon graphite ink formulation, which was printed onto a polyester flexible film (Autostat, UK 250 μm thickness) using the in-house fabricated screen print stencils (microDEK1760RS DEK, Weymouth). The percentage mass of MoS_{2PAR} was 5%, 10%, 15% and 20% for each of the three different MoS_{2PAR} sizes. The MoS_{2SUR} screen printed surfaces were cured for 30 min at 60 ºC, to remove trace solvents.

MoS_{2SUR} Surface Preparation. The MoS_{2SUR} printed surfaces were cut using scissors to form a 1 cm x 1 cm square. The surface was sterilized using 70% ethanol (Sigma-Aldrich, UK) for 10 min, and rinsed using a pipette and 2.5 mL of sterile distilled water at a 45˚ angle, then placed in a class II airflow cabinet to dry for 1 h.

Fourier Transform Infra-Red Spectroscopy (FTIR). A Thermo-Winslet Continuum FTIR microscope was used for analysis of the MoS_{2SUR}. The attachment used was a type A MCT detector. The aperture was used at 200 mm x 200 mm and the spectra of the MoS_{2SUR} was acquired using Omnic 5.2 software.

Inductively coupled plasma atomic emission spectroscopy (ICP-AES). The MoS_{2SUR} were placed into 15 mL Falcon tubes (Fisher Scientific, UK). Eight millilitres of sterile distilled water was added, and the samples were incubated at 37 ºC for 24 h with agitation (150 *rpm*). The solution was removed using a syringe and filtered using leur lock syringes (ThermoFisher, UK) with 0.2 μm sterile syringe filters (Starstead, UK). The solutions were analysed using an ICP–AES (Thermo scientific, iCAP6300 DUO, UK). The analysis parameters used were pump settings: flush pump rate – 50 *rpm*, analysis pump rate – 50 repetitions per min (*rpm*) and pump tubing – Tygon Orange / White. The source setting were as follows; RF power – 1250W, auxiliary gas flow – 0.5 L / min and nebuliser gas flow – 0.55 L / min with a sample flush time of 46 s ($n = 3$).

Scanning Electron Microscopy (SEM). The MoS_{2SUR} were mounted on aluminium SEM mounts (Agar Scientific, UK) with double-sided conducting carbon tabs (Agar Scientific, UK). The MoS_{2SUR}were characterised using a Zeiss Supra 40VP field emission gun scanning electron microscope (Zeiss, UK) and the following parameters; acceleration voltage -2.00kV, working distance 4.1 mm - 4.5 mm, SE2 detector, magnification at 10,000x.

Surface Roughness. Optical profilometry (Zemetrics, Germany), was used to determine the surface topography of the MoS_{2SUR}. Analysis of the surface roughness was carried out qualitatively via images, and quantitatively via *S* values; S_a, S_q and S_{pv} (arithmetical mean height, mean square roughness and mean maximum height respectively). The average peak and valley values from the line profiles were also taken (n = 10).

Water Contact Angle Measurements. Contact angle measurements were determined of the MoS_{2SUR} at room temperature using the sessile drop technique.[19] HPLC grade water (BDH, UK) at a drop size of 5 µL was deposited onto the horizontal substrata and the measurements were determined using a goniometer (KRUSS GMBH, Germany) (n = 3).

Stock Cultures. Stock cultures of *S. aureus* (NCTC 12981) and *P. aeruginosa* (PA01) were used for all microbiological assays. Stock solutions were stored in the freezer at -80℃. Cultures were thawed and inoculated onto tryptone soya agar (TSA) (Oxoid, UK) and incubated for 24 h at 37 ℃. Stock cultures were re-frozen immediately after use. For maintenance of bacterial physiology, inoculated plates were stored in the fridge at 4 ℃ and replaced every month.

Preparation of Bacterial Suspensions. A single colony of bacteria was added to 10 mL of tryptone soya broth (TSB) and vortexed for 10 s. The bacterial inoculum was incubated at 37 ℃ for 24 h in an orbital shaking incubator at 200 *rpm*. Bacterial cultures were centrifuged (Sigma-ALdrich 3-16L, UK) at 1721 *g* for 10 min, and the bacterial pellet was washed in 10 mL of 0.85% saline solution (Oxoid, UK) and vortexed for 10 s. The washing procedure was carried out twice. The bacteria were re-suspended to an optical density (OD) of 1.0 ± 0.1 at 540 nm using a spectrophotometer (Jenway 6305, UK). Colony forming units (CFU/ mL) were determined using serial dilutions and were 8.40 x 10^8 CFU/ mL for *S. aureus* and 2.88 x 10^8 CFU/ mL for *P. aeruginosa.*

Scanning Electron Microscopy. For visualisation of the single cell species, 100 µL of washed, single species bacterial suspensions were added to 10 mm x 10 mm silicon wafer surfaces (Montco Silicon Technologies Inc., USA) and dried for 30 min at room temperature in a class 2 microbiology cabinet. The single cell species, or bacterial biofilms were placed in 4% v/v glutaraldehyde (Agar Scientific, UK) overnight, then dehydrated in an absolute ethanol series of 30%, 50%, 70%, 90% and 100% v/v ethanol for 10 min. The samples were stored in a desiccator until they were sputter coated with a gold-palladium mix and imaged using SEM.

Retention Assay and Epifluorescence Microscopy. Three replicate MoS_{2SUR} were placed horizontally in a Petri dish and fixed using double sided tape. Thirty milliliters of standardized bacterial inoculation were added and incubated for 1 h at 37 ℃ without agitation.

Following incubation, the bacterial inoculum was removed and discarded using a sterile pipette. Non-adhered cells were gently removed from the MoS_{2SUR} with sterile distilled water (dH_2O) (2.5 mL), rinsing at a 45° angle for 5 s. The MoS_{2SUR} were dried in a class two airflow cabinet for 1 h before being stained with 0.03% acridine orange (Sigma-Aldrich, UK) dissolved in 2% glacial acetic acid (Sigma-Aldrich, UK). The stain was left on for 2 min before removing the MoS_{2SUR} and rinsing at a 45° angle for 5 s with 2.5 mL of dH_2O and air drying in the dark for 1 h. The substrata plus adhered microorganisms were visualized using epifluorescence microscopy and a F-View II black and white digital camera (Nikon Eclipse E600, Japan) using a 100 x oil immersion lens and a Nikon B-2A fluorescence filter. The MoS_{2SUR} were analysed using Cell-F software (Olympus, UK) (n = 3).

Multifractal Analysis to Determine Bacterial Coverage (Retention), Distribution, Density, Dispersion and Clustering. The epifluorescence images of the retention of the bacteria on the MoS_{2SUR} were analysed using multifractal analysis using the MATLAB®, Image Processing Toolbox® whereby the datasheets were converted to greyscale images. The properties of the typical theoretical multifractal datasets were computed for certain motifs using MATLAB.[24] Multifractal matrix (datasheets) of size 512 x 512 were computed by overlaying the given motifs one on top of another. In this case, a 2 x 2 matrix (motif) was overlayed (using iteration) to generate a 4 x 4 matrix image followed by an 8 x 8 matrix image until completion. The parameters α_{max} and α_{min} were used to measure the asymmetry of the curve ($\Delta\alpha_{AS}$). Symmetry of the $f(\alpha)$ curve indicates homogeneity and a lack of clustering. Asymmetry in the $f(\alpha)$ curve indicates clustering of gaps, if the curve is left skewed, and clustering of bright pixels, if the curve is right skewed. The height of the $f(\alpha)$ curve gives a measure of density of the pixels spread across the images, and the width gives a measure of dispersion. For the grayscale images used in this paper, D_0, the maximum value of the f(α) curve (when q = 0), gives a numerical value for the density of the cells on the surface, whilst $\Delta\alpha = \alpha_{max} - \alpha_{min}$, describes the heterogeneity of the cell spread on the surface. A skewed curve to the right indicated a clustering of the bacteria, whilst a left skewed curve gives an indication of clustering of gaps. The width of the f(α) curves gave a measure of dispersion of the bacteria. Aanalysis of the images was undertaken to determine the total retention of cells as a percentage (n = 3).

Crystal Violet Biofilm Assay. A bacterial inoculum was prepared for both bacterial species, as in the preparation of bacterial suspensions, but with the second broth re-suspension using tryptone soya broth (Oxoid, UK) instead of saline. A 12 well plate (Fisher Scientific, UK) was used for each bacterium and 1 mL of inoculated broth was added to each well. Sterile MoS_{2SUR} were added to the wells and negative controls were carried out. The plates were

wrapped in Parafilm (Fisher Scientific, UK) and incubated at 37 °C for 24 h. After incubation, the broth containing the bacteria was removed from the wells using a pipette, leaving the MoS_{2SUR} with attached biofilm. The MoS_{2SUR} were gently rinsed with sterile water at a 45° angle for 5 s to avoid removing the attached biofilm. One millilitre of 0.03% crystal violet solution (Prolab, UK) was added to each well and left to stand for 30 min before removing the crystal violet from the well using a pipette. The biofilm attached to the MoS_{2SUR} was rinsed with sterile water. Washing of the wells was repeated a further two times to ensure removal of all excess stain and loosely adhered cells. One millilitre of 33% glacial acetic acid (Fisher Scientific, UK) was added to each well and left to stand for 30 min. The optical density of each sample was measured at 540 nm against a blank of 33% glacial acetic acid ($n = 3$).[28]

Eukaryotic Cell Culture. Immortalised renal human proximal tubular (HK-2) cells (ATCC CRL-2190) were maintained in growth media medium (1:1 of Dulbecco's modified Eagle medium (DMEM): Ham's F-12 medium supplemented with 10% foetal bovine serum and penicillin/streptomycin (Life Technologies, UK). The cells were incubated at 37 ˚C in 5% CO_2 and the medium was refreshed every 48 h. At 80% confluence, the cells were rinsed with sterile phosphate buffered saline (PBS) and detached using a trypsin solution (Life Technologies, UK) to be counted by haemocytometer and seeded at required density in subsequent experiments.

HK-2 Cell Viability Assays. To evaluate the effect of leaching of MoS_2 on the viability of HK-2 cells, sterile MoS_{2SUR} were inserted into wells of 96 well plates. Then 200 µL of serum–free medium (SFM) (DMEM: Ham's F-12 medium supplemented with penicillin/streptomycin) were added to each well and the plates were incubated for 48 h at 37 °C in 5% CO_2. Control medium used as a negative control were generated by incubation of polyester flexible film substrates with 200 µL of SFM.

HK-2 cells were seeded in separate 96 well plates (Thermo Scientific, UK) at a density of 5,000 cells per well. The cells were incubated for 48 h in growth medium whereby reaching 80% confluency, and then they were growth arrested for 24 h in 200 µL of SFM. The medium was removed from each well and the cells were then exposed to 170 µL of SFM for 48 h at 37 °C in 5% CO_2. Following incubation, 9 µL of viability reagent WST-8 (tetrazolium-based cell counting kit-8, Tebu-Bio, UK) was added to each well and incubated for 1 h at 37 °C as per manufacturers recommendations. The absorbance of each well was measured at 450 nm and 650 nm using a plate reader (Thermo Scientific, UK) ($n = 6$).

Statistical Analysis. *p* values were calculated at the 95% confidence limits using student *t*-tests. Graphs were drawn in Microsoft Excel 2016. The results were reported as ± standard error. In all cases, $p < 0.05$ was considered statistically significant.

RESULTS

Fourier Transform Infrared Spectroscopy (FTIR) of the MoS_{2SUR}. The FTIR analysis of the MoS_{2SUR} demonstrated similar chemical moieties for all the MoS_{2SUR} (Figure 1). Analysis of the FTIR spectra extended from 4000 cm^{-1} to 400 cm^{-1}. Spectra between 3969 cm^{-1} – 3512 cm^{-1} were attributed to O-H stretching. N-H groups were determined in the 3405 cm^{-1} region. Other C dominated groups were demonstrated including C-H stretching, (2790 cm^{-1}, 2732 cm^{-1}, 736 cm^{-1}), O=C=O and C-O (2356 cm^{-1}, 1283 cm^{-1} respectively), C-N and C=N (2235 cm^{-1}, 1410 cm^{-1}, 1343 cm^{-1} and 2056 cm^{-1} respectively) were determined which may be indicative of the presence of the vinyl fillers. A graphite peak was observed at 2483 cm^{-1} for all the surfaces tested. Sulphur containing species were demonstrated at 1410 cm^{-1} and 1134 cm^{-1}. The molybdenum species were determined at 613 cm^{-1} and the Mo-S characteristic band was observed at 479 cm^{-1}. The bands in the lower frequency of the 400 cm^{-1} spectra may be characteristic of residual solvents used to make the graphitic inks.

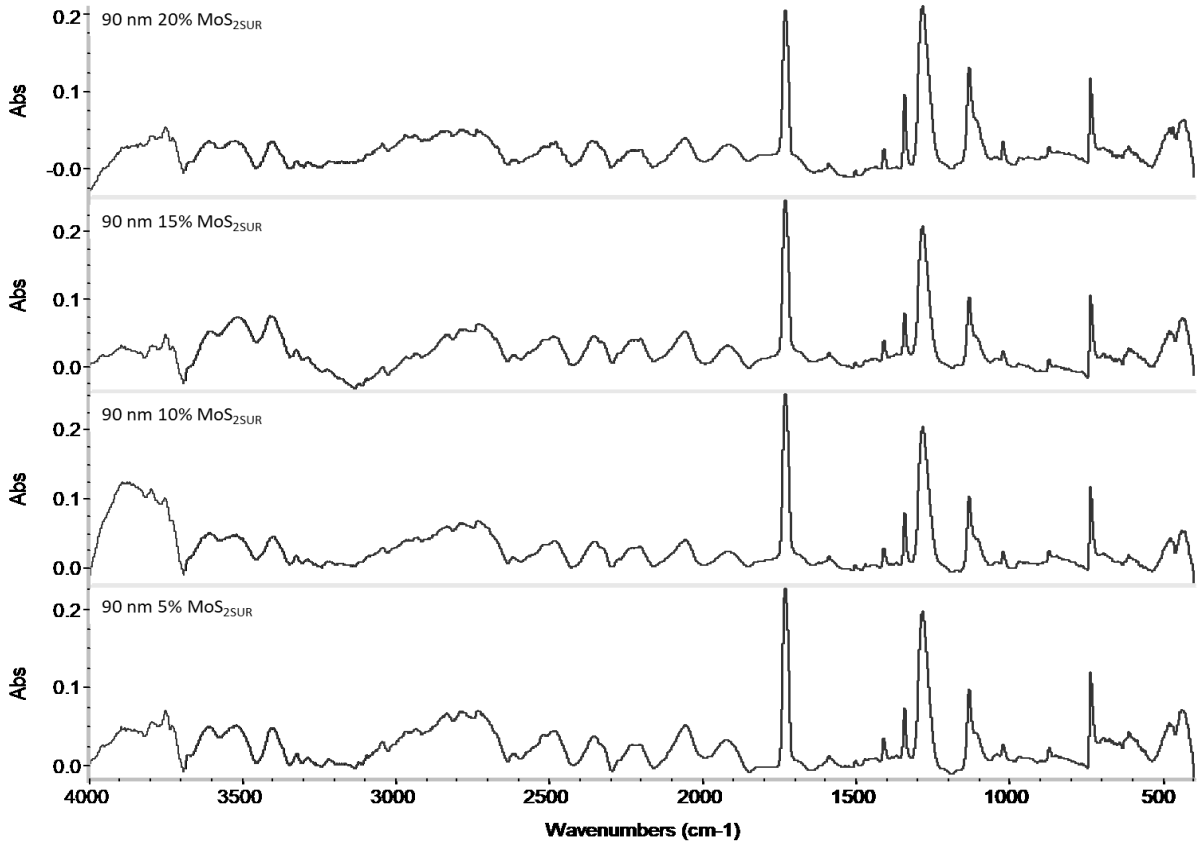

a)

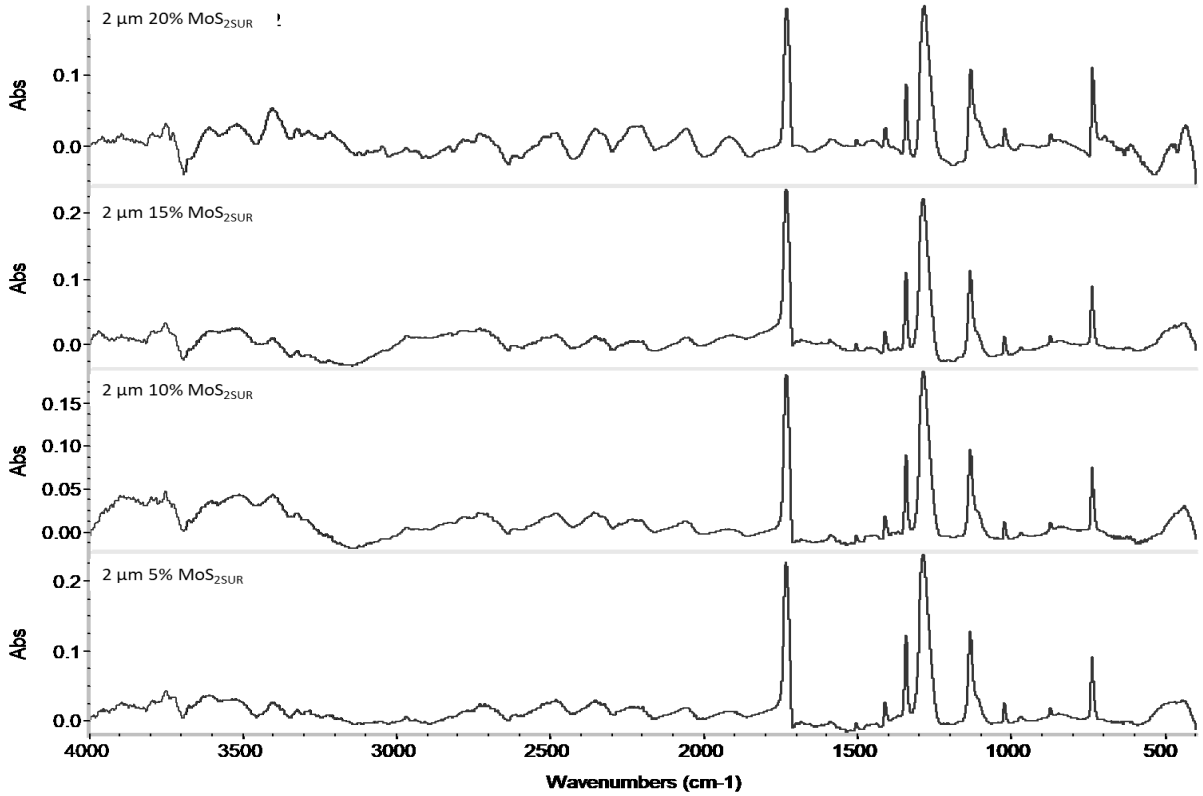
2 µm 20% MoS2SUR
2 µm 15% MoS2SUR
2 µm 10% MoS2SUR
2 µm 5% MoS2SUR
Abs
Wavenumbers (cm-1)
4000
3500
3000
2500
2000
1500
1000
500

b)

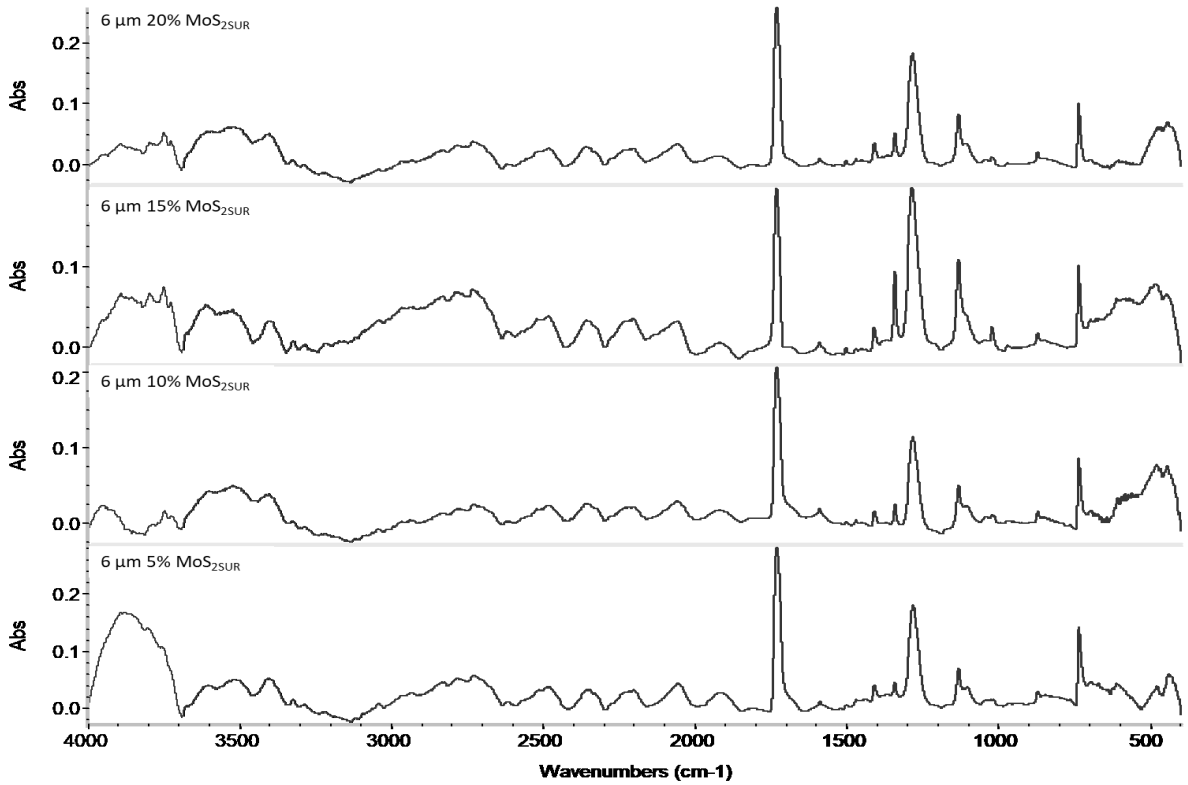
6 µm 20% MoS2SUR
6 µm 15% MoS2SUR
6 µm 10% MoS2SUR
6 µm 5% MoS2SUR
Abs
Wavenumbers (cm-1)
4000
3500
3000
2500
2000
1500
1000
500

c)

Figure 1. FTIR spectra of the MoS_{2SUR} incorporated with MoS_{2PAR} of 90 nm b) 2 µm and c) 6 µm at MoS_{2PAR} loadings of 5%, 10%, 15% and 20%.

Inductively Coupled Plasma Atomic Emission Spectroscopy. ICP-AES was carried out using the surfaces to determine the leaching of the ions. It was demonstrated that there was no significant difference in the leaching of either the molybdenum ions (Figure 2a), or the sulphur ions (Figure 2b) from the surfaces. For both molybdenum and sulphur ions, the amount detected leaching from the surfaces was considered to be negligible.

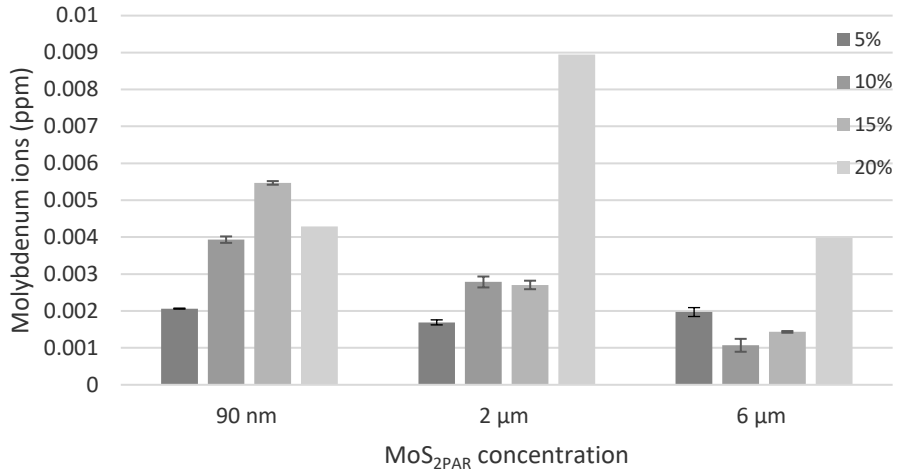

a)

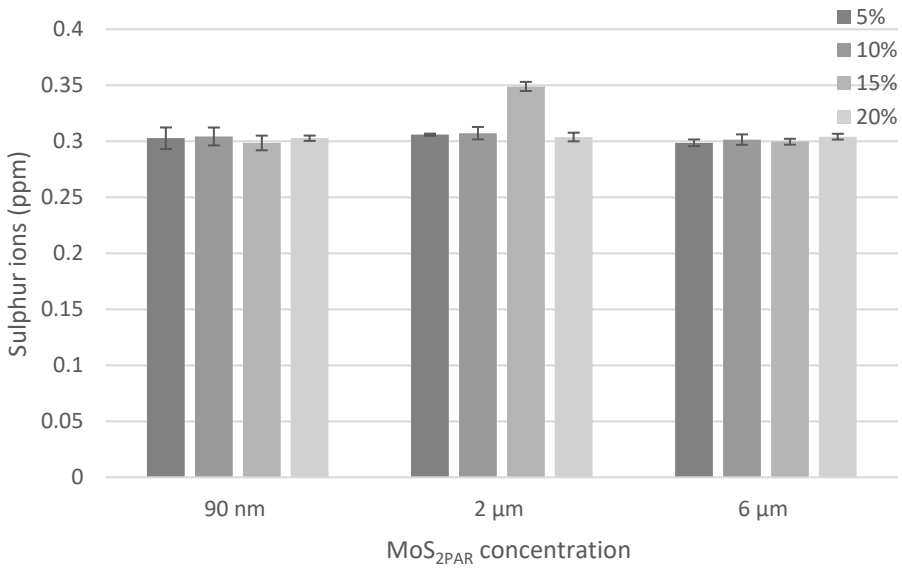

b)

Figure 2. ICP-AES of the MoS_{2SUR} demonstrating the leaching of molybdenum and sulphur ions (ppm).

Scanning Electron Microscopy of MoS_2. SEM was used to quantitatively analyse the MoS_{2SUR} at MoS_{2PAR} sizes of 90 nm, 2 µm and 6 µm, and at each concentration (5%, 10%, 15% and 20%). The shape of the MoS_{2PAR} were irregular in shape and size, and they were distributed throughout the matrix of the graphitic ink used to make the MoS_{2SUR}. The size of the MoS_{2PAR} varied and it was estimated that there was a 10% margin of error from the average MoS_{2PAR} size. The coverage of the MoS_{2PAR} was regular throughout the MoS_{2SUR}, but complete coverage of the MoS_{2SUR} was not evident. (Figure 3a - c). On the scanning electron micrographs a powder like coating was observed, which was the binder used to prevent the MoS_{2SUR} from flaking.

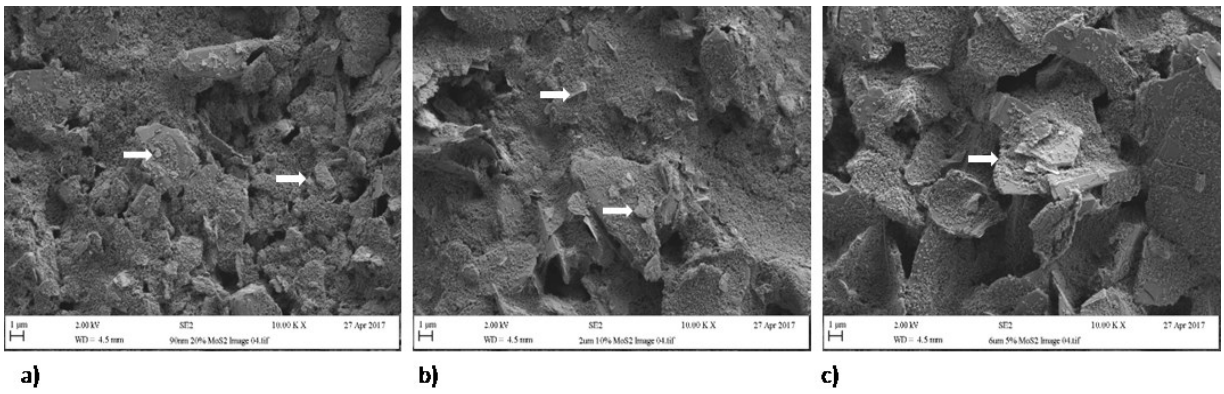

Figure 3. SEM images of the MoS_{2SUR} made with the a) 90 nm, b) 2 µm and c) 6 µm MoS_{2PAR}. The white arrows demonstrate the MoS_{2PAR} within the graphite ink matrix.

Surface Roughness Characterisation. Optical profilometery was carried out to determine the roughness (Figure 4 a-c) and shape of the topography of the MoS_{2SUR} (Figure 4d-f). It was demonstrated that there was complete coverage across the surfaces of the graphitic ink and in agreement with the SEM images, there were peaks on the topographical profiles corresponding to the protruding MoS_{2PAR}. It was evident from the linear profiles that the shape of the topographical features were sharper and more pointed for the MoS_{2SUR} made with the 90 nm MoS_{2PAR} (Figure 4b), than with the 2 µm MoS_{2PAR} (Figure 4d). The MoS_{2SUR} which incorporated the 6 µm MoS_{2PAR}, clearly demonstrated the largest and most square shaped surface topographical features (Figure 4f).

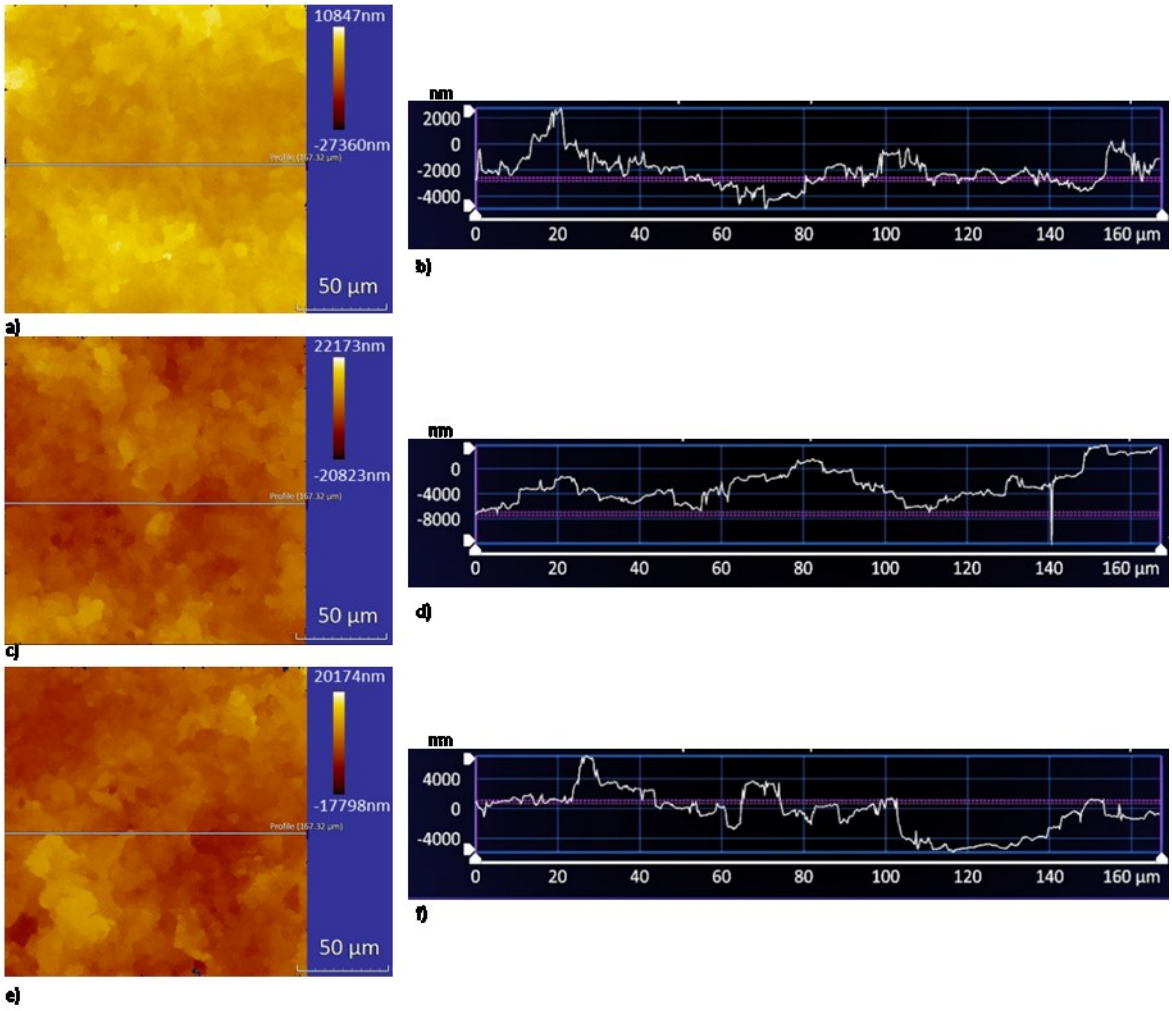

Figure 4. Optical profilometry maps and linear profiles demonstrating the surface coverage and shape of the topographic features on the MoS_{2SUR} a/b) 90 nm, c/d) 2 µm and e/f) 6 µm MoS_{2PAR} incorporated surfaces.

Line Profiles. The line profiles of the surface roughness were analysed to determine the size of the MoS_{2SUR} peaks and valleys (Table 1). The results showed that the MoS_{2SUR} fabricated with the 6 µm MoS_{2PAR} at 5%, 10%, 15% and 20% MoS_{2PAR} concentration possessed the largest average peak height (774.23 nm, 18.97 nm, 1097.14 nm and 1133.77 nm respectively) and the widest valleys (13.49 nm, 12.26 nm, 13.08 nm and 13.90 nm respectively). However, only the 6 µm peak height was significantly different to the other surfaces, except for the 6 µm MoS_{2SUR} with a 10% loading of MoS_{2PAR}, where a significant reduction in average peak height was demonstrated (18.97 nm). The lowest average peak height was observed on the 2 µm MoS_{2SUR} (27.46 nm, 17.74 nm, 16.53 nm and 16.7 nm respectively), whilst the 90 nm MoS_{2SUR} demonstrated the smallest average valley widths (10.22 nm, 12.26 nm, 10.22 nm and 11.04 nm respectively).

Table 1. Peak and valley widths and heights of the MoS_{2SUR} incorporated with 90 nm, 2 μm and 6 μm MoS_{2PAR} at concentrations of 5%, 10%, 15% and 20%.

Surface MoS_{2PAR} size and concentration	Largest peak height (nm)	Smallest peak height (nm)	Largest valley width (nm)	Smallest valley width (nm)
5% 90 nm	22.81 ± 2.9	0.01 ± 0.002	83.39 ± 6.2	10.22 ± 0.7
10% 90 nm	17.17 ± 2.1	0.02 ± 0.003	129.58 ± 10.1	12.26 ± 0.0
15% 90 nm	23.41 ± 3.5	0.01 ± 0.002	105.87 ± 7.3	10.22 ± 0.7
20% 90 nm	34.05 ± 4.3	0.01 ± 0.005	88.71 ± 4.7	11.04 ± 0.6
5% 2 μm	27.46 ± 5.4	0.01 ± 0.003	89.52 ± 10.6	10.22 ± 0.7
10% 2 μm	17.74 ± 2.3	0.01 ± 0.002	121.41 ± 9.4	12.26 ± 0.0
15% 2 μm	16.53 ± 0.8	0.02 ± 0.001	114.92 ± 5.7	10.34 ± 0.5
20% 2 μm	16.70 ± 3.0	0.02 ± 0.002	109.14 ± 4.9	12.26 ± 0.0
5% 6 μm	774.23 ± 293	0.64 ± 0.2	134.08 ± 8.8	13.49 ± 0.6
10% 6 μm	18.97 ± 2.7	0.01 ± 0.002	104.65 ± 6.0	12.26 ± 0.0
15% 6 μm	1097.14 ± 410	0.36 ± 0.1	123.04 ± 10.3	13.08 ± 0.5
20% 6 μm	1133.77 ± 146	0.21 ± 0.1	142.26 ± 8.8	13.90 ± 0.7

MoS_{2SUR} Roughness Parameters. Optical profilometry was used to obtain the roughness values of the MoS_{2SUR} (Figure 5). It was determined that for the MoS_{2SUR} of each MoS_{2PAR} size group (90 nm, 2 μm and 6 μm), when the concentrations of each MoS_{2PAR} size was compared (5%, 10%, 15% and 20%) no significant differences ($p > 0.05$) were demonstrated in the S_a (arithmetical mean height) (Figure 5a), S_q (mean square roughness) (Figure 5b) and S_{pv} (mean maximum height) (Figure 5c) values. However, when the MoS_{2SUR} in order of MoS_{2PAR} size were compared with one another, it was demonstrated that as MoS_{2PAR} size increased, so did the MoS_{2SUR} roughness. The 90 nm, 2 μm and 6 μm MoS_{2SUR} demonstrated the same trends in S_a, S_q and S_{pv} values, with the exception of the 6 μm MoS_{2PAR} sized MoS_{2SUR}, which demonstrated a different S_{pv} trend from those previously seen. The 2 μm MoS_{2SUR} at the 15% concentration demonstrated decreased S values (S_a of 1703.0 nm; S_q of 2119.2 nm and a S_{pv} of 31668.7 nm respectively), but these were not significantly different in comparison to the other 2 μm MoS_{2SUR} concentrations.

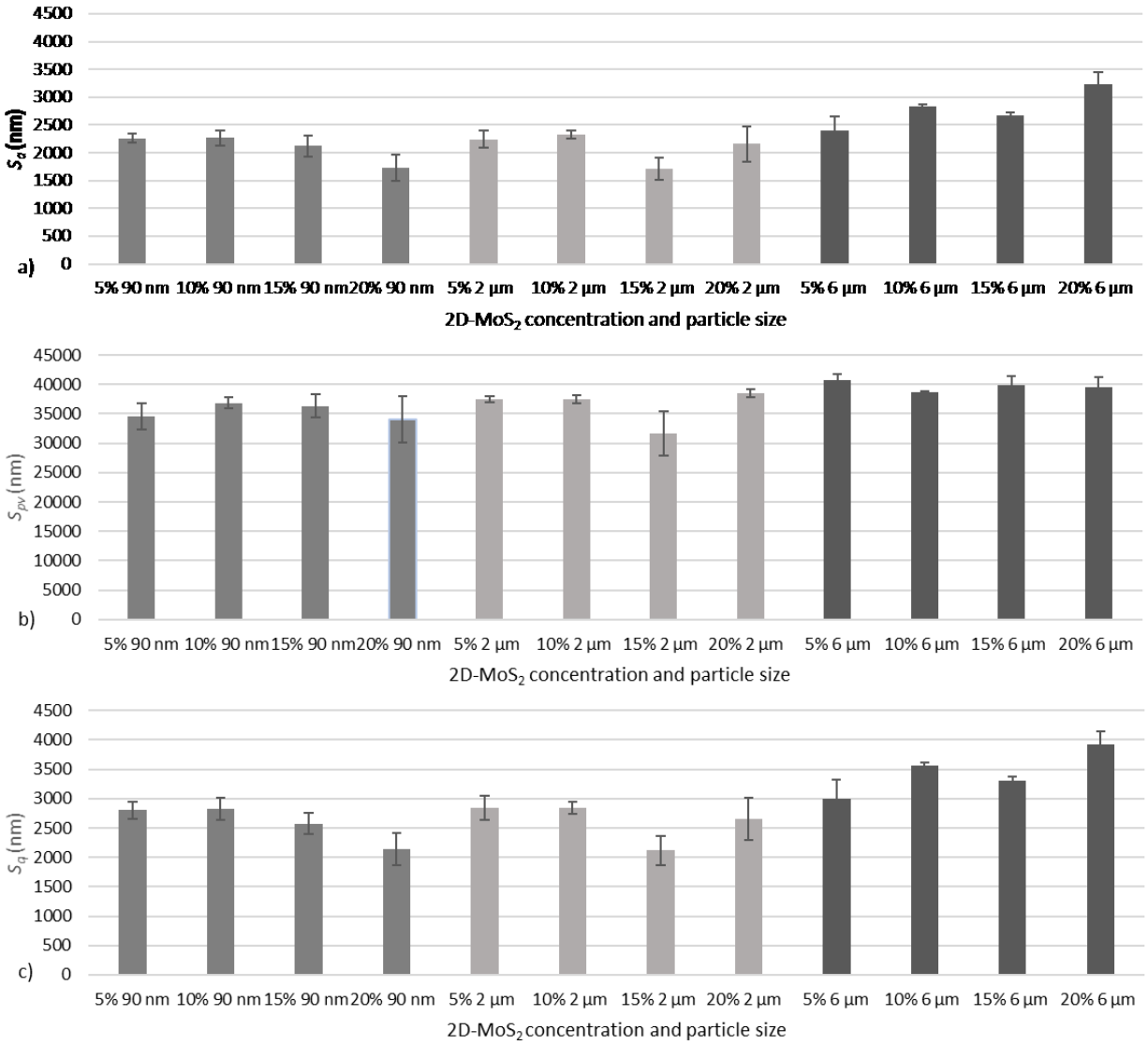

Figure 5. MoS_{2SUR} roughness parameters a) average MoS_{2SUR} roughness (S_a) values, b) MoS_{2SUR} mean square roughness values (S_q) and c) average maximum height of MoS_{2SUR} (S_{pv}) at increasing MoS_{2PAR} concentrations of 5%, 10%, 15% and 20%.

MoS_{2SUR} Water Contact Angles. Water contact angles were determined using the sessile drop technique (Figure 6). The MoS_{2SUR} demonstrated properties of a non-wettable nature, at the lowest concentrations of the MoS_{2PAR} in the MoS_{2SUR}. As MoS_{2PAR} concentration increased, the MoS_{2SUR} contact angle decreased and became more wettable. The 2 µm (100.0° – 106.7°) and 6 µm (96.3° – 106.7°) MoS_{2SUR} demonstrated significant differences when compared to the 90 nm (90.2° – 95.1°) MoS_{2SUR} (p = 0.003 and 0.005 respectively), whilst the wettability of the MoS_{2SUR} between the MoS_{2PAR} concentrations of the same MoS_{2PAR} sizes were not significantly different.

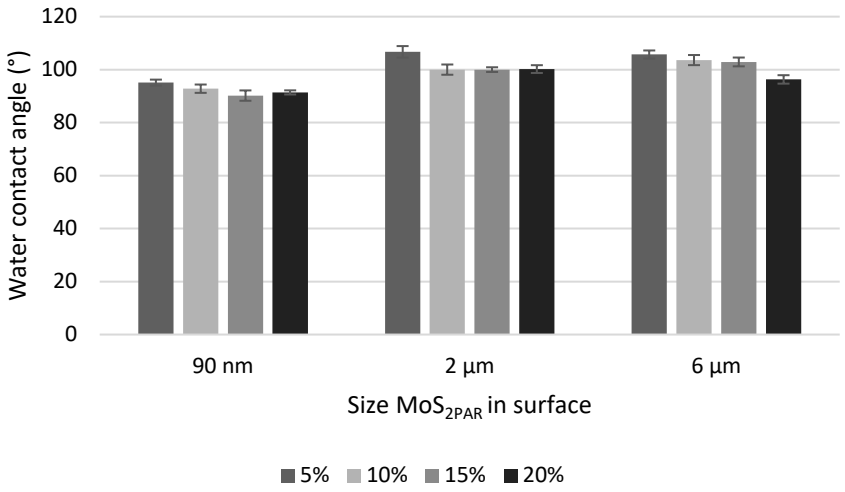

Figure 6. MoS_{2SUR} water contact angles incorporated with 90 nm, 2 µm and 6 µm MoS_{2PAR} at concentrations of 5%, 10%, 15% and 20%.

Bacteria. The bacteria used in this study were of different shapes and sizes (Figure 7). *P. aeruginosa* are rod shaped, 0.5 µm to 1 µm in width and 1 µm to 3 µm in length (Figure 7a). *S. aureus* is cocci in shape and around 0.5 µm to 1 µm in diameter (Figure 7b). Once the bacteria form biofilms, the cells cluster and are bound by exopolymeric substance as can be observed with *P. aeruginosa* (Figure 7c) and *S. aureus* (Figure 7d).

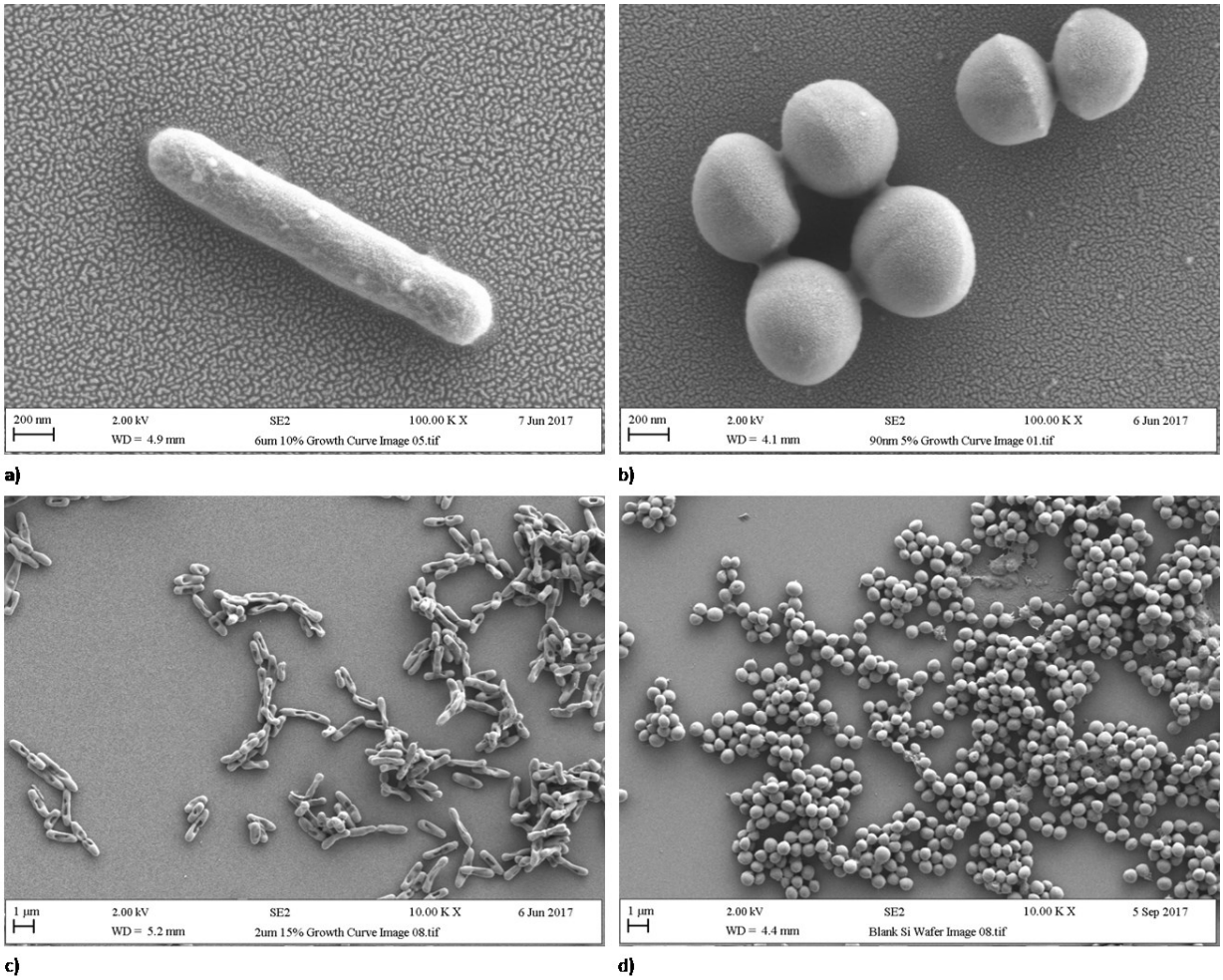

Figure 7. Morphology of different bacteria. Planktonic bacteria used in retention assays a) *P. aeruginosa* b) *S. aureus* and in biofilm formation c) *P. aeruginosa* and d) *S. aureus*.

Retention, Distribution, Density, Dispersion and Clustering of Bacteria Retained on MoS_{2SUR}**.** Epifluorescence microscopy and multifractal analysis was used to quantitatively determine the retention, density, dispersion and clustering of bacteria on the MoS_{2SUR}. The $f(\alpha)$ curves were used to determine the spreading parameters of the bacteria on the MoS_{2SUR} (ESI Figure 1). The curves for the *P. aeruginosa* retained on the 90 nm (ESI Figure 1a/d) and 6 µm (ESI Figure 1c/f) MoS_{2SUR} were skewed to the left-hand side demonstrating that the image was densely packed with cells. The longer leg of the $f(\alpha)$ curve (ESI Figure 1c) and increased skewness for the *P. aeruginosa* retained on the 6 µm MoS_{2SUR} evidenced that the number of cell clusters on the MoS_{2SUR} was greater, which was reflected in the microscopy image (ESI Figure 1f) when compared to the spread of the bacteria on the 90 nm MoS_{2SUR} (ESI Figure 1d). The *P. aeruginosa* retained on the 2 µm MoS_{2SUR} was skewed to the right-hand side demonstrating that the cells were more sparsely distributed, and this was reflected in the

microscopy image (ESI Figure 1e). The $f(\alpha)$ curves for the *S. aureus* were more symmetrical than for *P. aeruginosa* (ESI Figure 2) demonstrating that generally the density, dispersion and clustering elements of the microbial retention patterns were less pronounced that for the *P. aeruginosa*.

Retention of the bacteria across the MoS_{2SUR}. Multifractal analysis was used to quantify the retention, density, dispersion and clustering of the bacteria across the MoS_{2SUR} (Figure 8). An increase in retention of the bacterial cells (28.46% at 5%; 28.60% at 10% and 32.25% at 15% respectively) was shown at the 90 nm MoS_{2SUR} at each MoS_{2PAR} concentration (5%, 10% and 15%) with the exception of 20% MoS_{2PAR} (20.17%), and this followed the same pattern as the trend demonstrated in the S_a, S_q and S_{pv} values. On the 2 µm MoS_{2SUR}, the retention of *P. aeruginosa* the greatest numbers of bacteria retained were demonstrated on the 5% (55.30%) and 15% (37.84%) MoS_{2SUR}, whilst the least number of bacteria retained were demonstrated on the 10% (21.01%) and 20% (20.14%) MoS_{2SUR}. The retention patterns on these MoS_{2SUR} followed the opposite to the trend seen in the S_a, S_q and S_{pv} values of the MoS_{2SUR}. The MoS_{2SUR} at a MoS_{2PAR} of 6 µm demonstrated a decreasing trend of *P. aeruginosa* retention (45.97% at 5%. 45.11 at 10%; 26.72% at 15% and 24.30% at 20% respectively) as the concentration of MoS_{2PAR} increased along with an increase in MoS_{2SUR} roughness and wettability.

The retention of *S. aureus* followed a trend whereby, the percentage coverage of bacteria retained on the MoS_{2SUR} decreased with MoS_{2PAR} size, with the exception of the 5% 90 nm MoS_{2SUR}. The 2 µm MoS_{2SUR} demonstrated the lowest *S. aureus* retention on the 5%, 10% and 15% MoS_{2PAR} MoS_{2SUR} (23.44%, 20.80% and 14.69% respectively) when compared to the 90 nm and 6 µm MoS_{2PAR} MoS_{2SUR} at the same concentration of MoS_{2PAR} loadings. The retention of *S. aureus* on the MoS_{2SUR} demonstrated the overall highest retention on the 5% and 10% 6 µm MoS_{2PAR} MoS_{2SUR} (52.24% and 52.37% respectively). The lowest retention was demonstrated on the 6 µm MoS_{2PAR} size surface with a 20% concentration (6.11%) (Figure 8a). Across all MoS_2 MoS_{2PAR} sizes tested, the 20% MoS_2 concentrations demonstrated the lowest *S. aureus* retention (11.98% at 90 nm; 13.84% at 2 µm and 6.11% at 6 µm respectively). The retention of the bacteria on the MoS_{2SUR} followed the same trend as the S_a, S_q and S_{pv} values for the MoS_{2SUR} made with the 90 nm MoS_{2PAR}, and for the 2 µm and 6 µm MoS_{2PAR} MoS_{2SUR}, the increase in MoS_{2SUR} wettability, also resulted in a decrease in bacterial retention.

Density of bacteria across the MoS_{2SUR}. The $f(\alpha)$ curves were used to calculate the density of the *P. aeruginosa* across the MoS_{2SUR} (Figure 8b). None of the MoS_{2SUR} made with

the different MoS_{2PAR} sizes (90 nm, 2 μm and 6 μm) demonstrated trends in the density of the *P. aeruginosa* that could be related to the MoS_{2SUR} properties. The 90 nm MoS_{2SUR} demonstrated the lowest average density across all MoS_{2PAR} concentrations (range 1.85 to 1.88), but only the density of the bacteria across the 15% MoS_{2SUR} was significantly different. For the 2 μm MoS_{2SUR} there was only a significant difference between the highest density on the 5% MoS_{2SUR} (1.89) and the lowest density on the 10% (1.87) MoS_{2SUR}. On the 6 μm MoS_{2SUR}, the highest level of *P. aeruginosa* density (1.91 at 15% was also significantly different to the lowest level of density demonstrated on the 20% MoS_{2SUR} (1.87%).

When comparing the measurements on the MoS_{2SUR} made with the 90 nm MoS_{2PAR} size, the density of the *S. aureus* increased (1.89 at 5%; 1.90 at 10% and 1.90 at 15%) with the exception of the 20% MoS_2 (1.85) (Figure 8b). The 2 μm MoS_{2SUR} demonstrated a trend whereby *S. aureus* density decreased marginally (1.9 at 10%; 1.9 at 15% and 1.89 at 20%) with increasing MoS_{2PAR} concentration, with the exception of the 5% MoS_{2SUR} (1.87). At the largest MoS_{2PAR} size of 6 μm, the density of bacteria remained constant (1.88 at 5%; 1.87 at 15% and 1.87 at 20%) with the exception of 10% MoS_{2PAR} (1.91) concentration, although this was not statistically signifcant (p<0.05). In summary, the greatest density of *S. aureus* was demonstrated on the 6 μm 10% MoS_{2PAR} concentration MoS_{2SUR} and lowest on the 90 nm MoS_{2PAR} size 20% concentration MoS_{2SUR}, but overall bacterial density did not demonstrate a trend with MoS_{2SUR} properties.

Distribution of the bacteria across the MoS_{2SUR}. On all the MoS_{2SUR}, *P. aeruginosa* were heterogeneously spread across the MoS_{2SUR}. The most heterogeneously spread bacteria were on the 90 nm MoS_{2PAR}, 15% MoS_{2SUR} (0.66), and on the 6 μm, 5% MoS_{2PAR} (0.67) and 10% MoS_{2PAR} (0.69) MoS_{2SUR} (Figure 8c). Only on the 6 μm MoS_{2SUR} did *P. aeruginosa* demonstrate a trend between the surface properties and bacterial dispersion, whereby as the MoS_{2SUR} increased their MoS_{2PAR} size and became more wettable, so the bacteria became more dispersed.

S. aureus demonstrated an increase in dispersion (0.67 at 5%; 0.70 at 10%; 0.78 at 15% and 0.95 at 20% respectively) (Figure 8c) on the 6 μm MoS_{2SUR} as MoS_{2PAR} concentrations increased. This was not observed with the *S. aureus* on the 90 nm or 2 μm MoS_{2SUR}, and the 90 nm and 2 μm MoS_{2PAR} sizes demonstrated no significant differences in the dispersion of bacteria. With regards to the MoS_{2SUR} properties, the MoS_{2SUR} made with the 90 nm and 2 μm MoS_{2PAR} did not demonstrate a trend with the S_a, S_q, S_{pv} or wettability values. However, the 6

μm MoS_{2SUR} demonstrated an increase in bacterial dispersion with increased MoS_{2SUR} roughness.

Clustering of bacteria across the MoS_{2SUR}. Clustering of the bacteria across the MoS_{2SUR} demonstrated that on the 90 nm MoS_{2SUR}, the clustering of *P. aeruginosa* decreased with the concentration of MoS_{2PAR} loading (0.03 to 0.48). A different trend was demonstrated on the 2 μm MoS_{2SUR}, whereby the clustering of the *P. aeruginosa* on the 5% MoS_{2SUR} (0.77) was significantly different to the other MoS_{2SUR} (0.11 at 5%, 0.23 at 15% and 0.12 at 20%). Only on the 6 μm MoS_{2SUR} was a clear trend observed, whereby *P. aeruginosa* clustering decreased with increased MoS_{2PAR} loadings (0.94 at 5%, 0.75 at 10%, 0.31 at 15% and 0.04 at 20%) (Figure 8d). Overall, *P. aeruginosa* demonstrated less trends in their distribution across the MoS_{2SUR} related to the MoS_{2SUR} properties than did *S. aureus*.

The underlying MoS_{2PAR} size and concentration produced different trends in the *S. aureus* clustering patterns on the MoS_{2SUR} (Figure 8d). On the 90 nm MoS_{2SUR}, clustering of the *S. aureus* was greatest on the 10% MoS_{2SUR} (0.83), and lowest on the 20% MoS_{2SUR} (-0.24), whilst on the 2 μm MoS_{2SUR}, clustering of the bacteria was greatest on the 10% (0.56), but lowest on the 15% MoS_{2SUR} (0.09). Only the 6 μm MoS_{2SUR} demonstrated decreased clustering of the *S. aureus* with increased MoS_{2PAR} size and concentration (1.07 at 5%, 0.94 at 10%, 0.36 at 15% and -0.68 at 20% respectively).

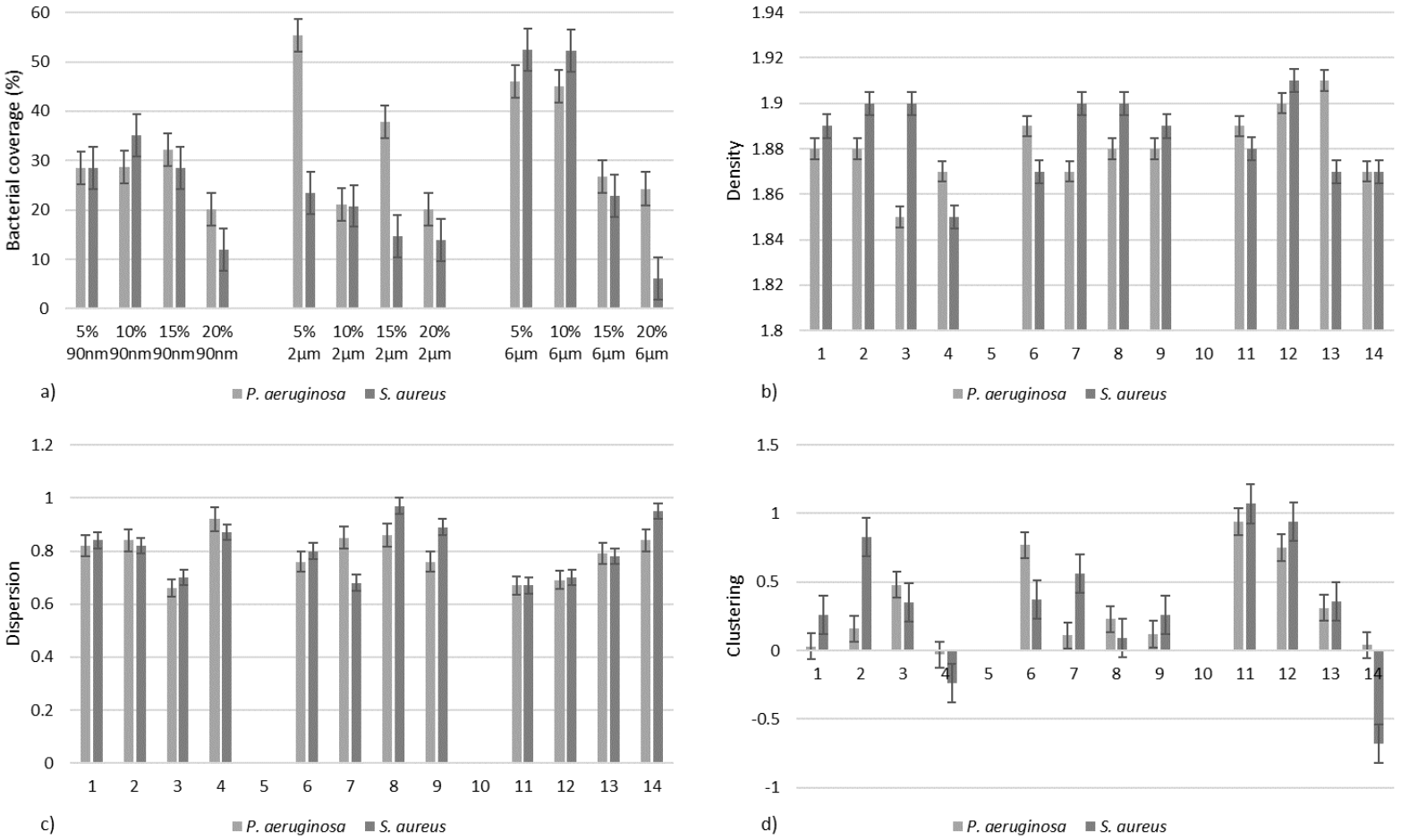

Figure 8. Pattern of *P. aeruginosa* and *S. aureus* a) retention (percentage coverage) b) density, c) dispersion and d) clustering across the MoS_{2SUR} with MoS_{2PAR} loadings of 5%, 10%, 15% and 20%.

Crystal Violet Biofilm Assay. The 2 µm MoS_{2SUR} were tested to determine if they had an effect on bacterial biofilm formation over 24 h (Figure 9). The MoS_{2SUR} demonstrated a reduction in biofilm formation for *S. aureus* (1.27, 1.61, 1.15 and 0.93) and *P. aeruginosa* (1.53, 1.53, 1.33 and 1.03) with increasing MoS_{2PAR} size incorporated into the MoS_{2SUR}. The total biofilm growth was reduced on MoS_{2SUR} made with increasing MoS_{2PAR} sizes and concentration of MoS_2 by 28.5% for *S. aureus* and 34.8% for *P. aeruginosa.* These MoS_{2SUR} also demonstrated a corresponding trend of increased wettability with decreased biofilm formation.

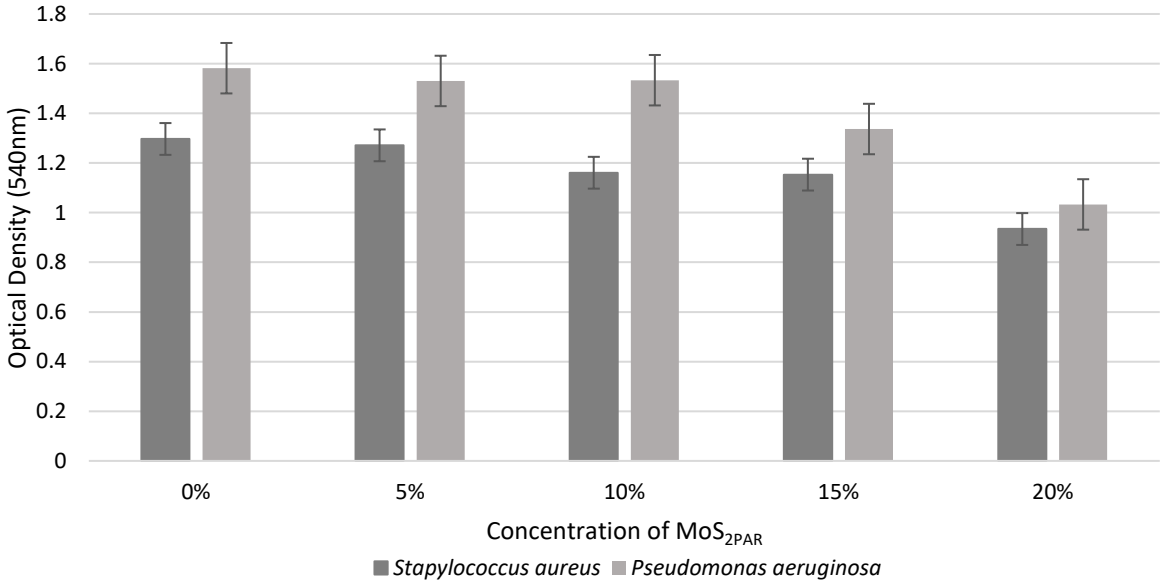

Figure 9. Biofilm of *S. aureus* and *P. aeruginosa* against MoS_{2SUR} at increasing concentrations of MoS_{2PAR} (5%, 10%. 15% and 20%) (n = 3).

HK-2 Cell Cytotoxicity. Immortalised renal human proximal tubular cells (HK-2) were used to determine the cytotoxicity of the MoS_{2SUR}. Cell viability was measured after 48 h of exposure of cells to SFM incubated with the control surfaces, or the 90 nm, 2 µm or the 6 µm MoS_{2SUR} at a concentration of 20% MoS_{2PAR} (Figure 10). The results demonstrated a decrease in HK-2 cell viability with increasing MoS_{2PAR} size in the MoS_{2SUR} (102.4%, 99.1% and 83.9% for 90 nm, 2 µm, and 6 µm surfaces respectively), in comparison to the control. The reduction in viability was significant only in response to media incubated with 6 µm MoS_{2SUR}, when compared the control, and the 90 nm MoS_{2PAR} sized MoS_{2SUR}.

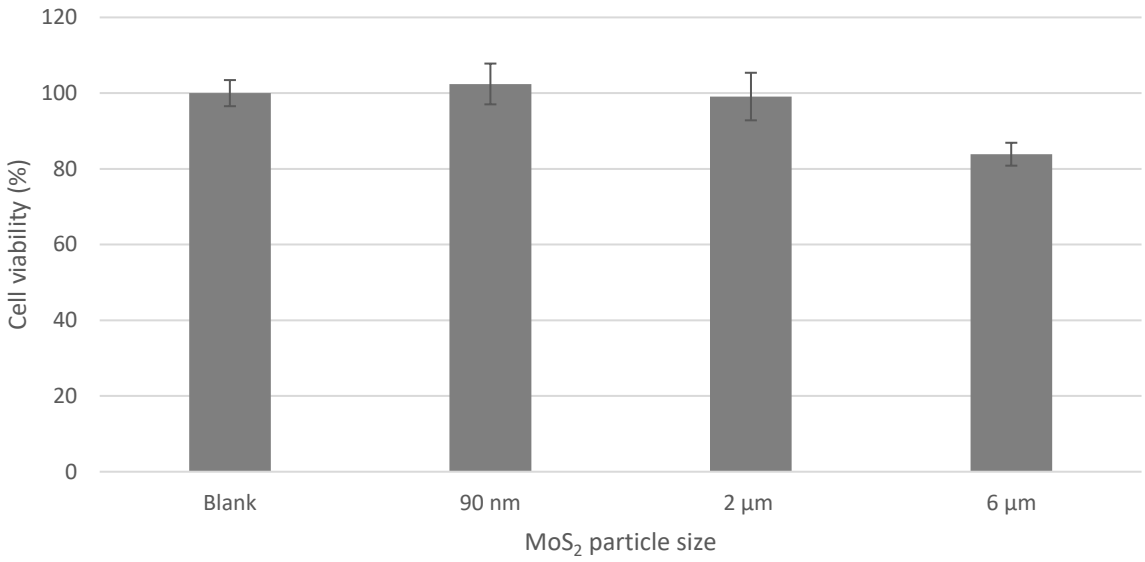

Figure 10. The effect of molybdenum and sulphur leached from MoS_{2SUR} on HK-2 cell viability. Cells were incubated for 48 h with SFM exposed to a control or MoS_{2SUR} at 20% MoS_{2PAR} concentration, and MoS_{2PAR} sizes of 90 nm, 2 µm or 6 µm. Cell viability was expressed as a percentage of the control cells. MoS_{2SUR} of 6 µm sized MoS_{2PAR} demonstrated significant reductions in HK-2 cell viability in comparison to the control ($p = 0.006$) and the 90 nm MoS_{2PAR} ($p = 0.013$) ($n = 6$).

DISCUSSION

Due to the prevalent issue of bacterial retention, which subsequently leads to biofilm formation, the food, water and medical industries require novel ways to combat biofouling.[25,26,29,30] A range of 2D materials have gained significant attention in recent years for their unique physical and chemical properties.[18] The ICP-AES results demonstrated that there was negligible leaching of the molybdenum or sulphur from the MoS_{2SUR}, thus consolidating the fact that, the mechanism of action of bacterial retention and biofilm formation was an effect determined by surface properties, rather than being due to a biocidal action. The FTIR spectra of the MoS_{2SUR} demonstrated that the spectral peaks for the MoS_{2PAR} and other components such as the graphite, binder and residual solvents in the graphitic ink were detected. The shifts in the peaks may be due to binding of other molecules in the MoS_{2SUR} to the components of the graphitic ink. In agreement with the results in the FTIR, previous work had analysed the MoS_{2SUR} using X-ray Diffraction Spectroscopy, X-ray Photoelectron Spectroscopy and Raman Spectroscopy analysis had demonstrated the chemistry of the MoS_{2SUR} and the robustness of the MoS_{2SUR} when used as electrodes[31]. The results were found

to demonstrate that the surfaces exhibited no degradation in current when used in over a 1000 repeat scans, thus supporting the stability of these MoS_{2SUR} over time.[31] The FTIR analysis and SEM images demonstrated that the MoS_{2SUR} were chemically heterogeneous. The thickness of MoS_{2SUR} was dependent on the printing parameters and ink viscosity, but previous work had demonstrated that the thickness of the MoS_{2SUR} was 13.5 ± 1.5 microns.[31] The MoS_{2SUR} demonstrated different MoS_{2PAR} size affected surface wettability and roughness, whereas changes of MoS_{2PAR} concentration only affected surface wettability.

The properties of a surface can influence the retention of bacteria and hence subsequent biofilm formation.[32] Different facets of the MoS_{2SUR} properties, and also the bacterial shape were found to affect the bacterial retention to the MoS_{2SUR} and these included the shape and size of the MoS_{2SUR} features and microorganisms, the different MoS_{2PAR} sizes incorporated into the MoS_{2SUR} and the concentration of the MoS_{2PAR} in the MoS_{2SUR}. The MoS_{2SUR} with the smaller topographical shaped features, and the concentration of the MoS_{2PAR} incorporated into the MoS_{2SUR} influenced the pattern of retention of the *S. aureus* bacteria, with some trends in retention seen for the *S. aureus* on the MoS_{2SUR} made with the 90 nm and 2 µm MoS_{2PAR}. *P. aeruginosa* are rod shaped bacteria (1 µm diameter by 1 µm – 3 µm length) and are larger than the cocci shaped *S. aureus.* in size (0.5 µm – 1 µm diameter). The smaller MoS_{2SUR} features of the MoS_{2SUR} made with the 90 nm or 2 µm MoS_{2PAR} may have enabled the smaller bacteria to be retained. This is one explanation as to why increasing the concentrations of the MoS_{2PAR} in the MoS_{2SUR} would result in the different behaviour of the bacteria. Although there is controversy regarding the influence of surface topography on bacterial retention, in agreement with our work, it has demonstrated that the size of the surface features can significantly affect bacterial retention.[6,33-35]

The increase in the MoS_{2PAR} used to make the MoS_{2SUR} increased the MoS_{2SUR} topography and wettability which resulted in the greatest bacterial reduction on the roughest, most wettable MoS_{2SUR}. The water contact angle of MoS_{2SUR} has previously been reported to be between 75.8° and 88.37°.[36-38] However, graphite is known to be a less wettable material, with a water contact angle between 75°- 95°.[39] Thus, the increase of the MoS_{2SUR} wettability with an increase in the concentration in the MoS_{2PAR} in the MoS_{2SUR} would be expected. As the MoS_{2SUR} become more wettable with increasing MoS_{2PAR} concentration, if the physicochemical forces between the bacteria and the MoS_{2SUR} become similar, this may result in repulsive interactions and hence the MoS_{2SUR} with the higher concentrations of MoS_{2PAR} would repel the bacteria. This may explain why increasing the concentrations of the MoS_{2PAR} in the MoS_{2SUR} would result in the different behaviour of the bacteria. In agreement with our

work it has been suggested that a way to reduce fouling, particularly on membranes is increase the surface hydrophilicity.[40]

As the MoS_{2SUR} topography and wettability increased with increasing MoS_{2PAR} size and concentration, the bacteria became more heterogeneously dispersed and less clustered across the MoS_{2SUR}. *P. aeruginosa* demonstrated different patterns of retention, distribution, density, dispersion and clustering compared to the *S. aureus* suggesting that the interaction of the different MoS_{2SUR} properties in conjunction with the morphology and physiology of the cells had a role to play.

Although much work has been carried out on the antibacterial properties of 2D materials, very little work has been carried out on the capabilities of such materials to impede biofouling. Alam et al., (2018) demonstrated that MoS_{2SUR} performed as well as graphene oxide in reducing *Escherichia coli* adherence to MoS_{2SUR}.[22] which was suggested to be due to the lowered amount of functional groups on the MoS_{2SUR}. Using QCM-D when natural organic matter was injected onto MoS_{2SUR} and graphene oxide surfaces, a lesser frequency shift was observed on the MoS_{2SUR}, indicating that the MoS_{2SUR} would be less prone to fouling.[22]

The advantage of using MoS_{2SUR} is that they are cheap to produce and generally considered non-toxic and since they are antifouling rather than antimicrobial, they do not require the addition of other chemicals or metallic elements that may result in an increase in their toxicity profiles. MoS_{2SUR} may also be more beneficial than other 2-D material surfaces since they been reported to contain less functional groups. Since the functional groups in graphene oxide forms hydrogen bonds with the lipopolysaccharides of Gram-negative bacteria, such as *P. aeruginosa*, the lack of functional groups on MoS_{2SUR} may result in lowered bacterial:surface interactions.[41,42] There is also a need to look for antifouling surfaces that do not contain metals. Although metals are a regular component of antifouling coatings, such as partially reduced graphene oxide/silver in nanocomposite and zinc-graphite composite coatings, there is concern over the toxic effects of these materials.[11,12] Another factor is the uncontrolled use of silver as an antimicrobial in a wide range of applications and products and concerns are now being raised regarding the development of bacterial resistance to silver.[43] Thus the development of such surfaces that impede bacterial retention and biofilm formation with lowered toxicity profiles is highly advantageous.

Evaluation of the biofilm reducing properties of the MoS_{2SUR} demonstrated the same trend for each bacterial type, whereby a decrease in biofilm formation for *P. aeruginosa* and *S. aureus* was positively correlated with an increase in the concentration of MoS_{2PAR} in the $MoS_{2SUR.}$ The overall biofilm growth was reduced with increasing MoS_{2PAR} sizes and

concentration of MoS_{2SUR} by 34.8% for *P. aeruginosa* and 28.5% for *S. aureus*. This may have resulted since as the biofilm forms on the surface, exopolymeric substance (EPS) is produced by the cells which will coat both the surface of the MoS_{2SUR} and the bacterial cell walls, resulting in similar chemistries on both the different types of cells. The exopolymeric substance have different patches or domains that can have a hydrophobic, hydrophilic, and positively or negatively charged nature, and the covering of the bacteria and MoS_{2SUR} may have mitigated any bacterial:surface interaction effects.[44,45] This is one mechanism which may explain why in the biofilm study, although different shaped and sized cells were used, they are seen to act in the same manner. The differences in the amount of biofilm produced on the MoS_{2SUR} may be therefore due to the initial bacterial load on the MoS_{2SUR}. This correlates with the retention values whereby the least amount of retained bacteria was observed on the surfaces loaded with the greatest concentration of MoS_{2PAR}. In agreement with the results presented in this work, Yuwen et al., (2018), demonstrated that increasing the concentration of molybdenum within a hybrid surface, significantly reduced the presence of *S. aureus* biofilms.[46] The results from this study clearly demonstrate that the retention of bacteria on surfaces and biofilm formation are influenced by different phenomenon.

The use of cell viability assays for investigating cytotoxicity of surfaces *in vitro* is of importance, particularly when such surfaces have a potential to be used in the healthcare, water and food sectors. Despite the existing uses of 2D materials in biomedical applications, research into their toxicity in human cell lines is limited, with differences in testing methods, or without sufficient materials characterisation.[47] Studies on two dimensional materials, such as reduced graphene oxide and MoS_2, have previously demonstrated conflicting effects on cell cytotoxicity in mammalian cell lines.[48,49]

An *in vitro* rat endothelial cell model testing the cytotoxic effects of media incubated with MoS_2 nanosheets demonstrated that increasing MoS_2 concentrations did not impair the cell viability.[50] Furthermore, some of the MoS_2 concentrations tested increased proliferation of the cells after 24 h of incubation. The cell viability in their study was measured using sulforhodamine B assay by quantifying the cellular protein content in living cells, pre and post MoS_2 interaction. Studies utilising the WST-8 viability assay have demonstrated that MoS_2 does not impair the cell viability of human embryonic kidney cells and lung epithelial cells.[50,51] Similar results were observed in this study, where media incubated with 90 nm and 2 µm MoS_{2PAR} were non-toxic to human kidney cells (HK-2) over a 48 h period of incubation. Furthermore, the viability of HK-2 cells exposed to the 90 nm MoS_{2PAR} was increased as compared to the control media, possibly due to increased

proliferation and cell growth. In contrast, media incubated with the 6 µm MoS_{2PAR} significantly reduced HK-2 cell viability. However, some evidence suggests that the size of the MoS_{2PAR} may have an effect on cell viability.[52] Chng and Pumera, (2015), have demonstrated a correlation between the surface area of MoS_{2PAR} and their cytotoxic effects in A549 human lung epithelial cells.[53] Similar effects were observed by Zhang et al, (2017), where the flake size of similar 2D materials correlated with cell death in NIH 3T3, HCoEpiC and 293T cell lines.[54] The reduction in viability is attributed to an increase in reactive oxygen species generation, which correlated with an increase in the flake size of the particulates. Therefore, it is likely that the cytotoxic effects of the 6 µm MoS_{2SUR} observed in this study are due to an increased reactive oxygen species generation, due to increased surface MoS_{2PAR} size.

The results from this study demonstrated that MoS_{2SUR} have the potential to impede surface fouling. Such surfaces may be useful for use for specific applications within certain industries or healthcare where biofilm proliferation is an issue.

CONCLUSION

This work demonstrated that increasing the MoS_{2PAR} size, resulted in MoS_{2SUR} that had the least sharp surface topographies, with wider width valleys. The 6 µm MoS_{2SUR}, demonstrated the most dominant effects on both bacteria in terms of retention whereby, the increase in the concentration of the MoS_{2PAR} in the MoS_{2SUR} resulted in increased surface wettability and roughness but a decrease in bacteria retention and clustering and an increase in bacterial dispersion. Surfaces with smaller features and increased wettability had an effect on the retention of *S. aureus,* due to the smaller bacteria being able to fit into the smaller surface features. When the efficacy of the MoS_{2SUR} was tested against the biofilms, it was demonstrated that the amount of bacterial loading influenced the amount of biofilm formation. These results suggest that the surface properties of materials influenced microbial retention, and the amount of initial bacterial load influenced biofilm formation. Such bacterial retention and biofilm reducing MoS_{2SUR} may be further developed for use in industries whereby surface biofouling is an issue.

AUTHOR INFORMATION

Corresponding Author

*K. A. Whitehead, Manchester Metropolitan University, UK. Tel: +44 161 247 1157. E-mail address K.A.Whitehead@mmu.ac.uk

ORCID

Mohsin Amin 0000-0003-3873-8820, Samuel Rowley-Neale , Liliana Shalamanova 0000-0003-4606-2234, Stephen Lynch 0000-0002-4183-5122, Joels T. Wilson-Nieuwenhuis 0000-0002-8906-4304, Mohamed El Mohtadi 0000-0002-5707-6415, Craig E. Banks 0000-0002-0756-9764 and Kathryn A. Whitehead 0000-0001-6001-6686

AUTHOR CONTRIBUTIONS

KW developed the idea conceptualisation and drafted the final manuscript. MA, SR-N, LS, SL, JW-N and ME-M contributed to the material and manuscript preparation, data collection and analysis. CB and SR-N lead the surface design. All authors read and approved the final manuscript.

CONFLICT OF INTERST

There is no conflict of interest in this work.

FUNDING

There are no funders to report.

SUPPLEMENTARY INFORMATION

- $f(\alpha)$ curves derived for the a) 90 nm, b) 2 µm and c) 6 µm MoS_{2PAR} incorporated into the MoS_{2SUR} derived from the corresponding images following the bacterial retention assays of *P. aeruginosa* on the d) 90 nm, b) 2 µm and c) 6 µm surfaces demonstrating the mathematical information used to determine the percentage coverage, density dispersipon and clustering of *P. aeruginosa.* Error bars are representative of 50 µm.
- $f(\alpha)$ curves derived for the a) 90 nm, b) 2 µm and c) 6 µm MoS_{2PAR} loaded MoS_{2SUR} derived from the corresponding images following the bacterial retention assays of *S. aureus* on the d) 90 nm, b) 2 µm and c) 6 µm surfaces demonstrating the mathematical information used to determine the percentage coverage, density dispersipon and clustering of *S. aureus.* Error bars are representative of 50 µm.

REFERENCES

(1) Whitehead, K.; Olivier, S.; Benson, P.; Arneborg, N.; Verran, J.; Kelly, P. The Effect of Surface Properties of Polycrystalline, Single Phase Metal Coatings on Bacterial Retention. Inter. J. Food Microbiol. 2015, 197, 92-97

(2) Whitehead, K. A.; Verran, J. The Effect of Substratum Properties on the Survival of Attached Microorganisms on Inert Surfaces. In: Marine and Industrial Biofouling 2009, 4, 13-33

(3) Hood, S.; Zottola, E. Adherence to Stainless Steel by Foodborne Microorganisms During Growth in Model Food Systems. Inter. J. Food Microbiol. 1997, 37, 145-153

(4) Bos, R.; van der Mei, H.; Busscher, H. Physico-Chemistry of Initial Microbial Adhesive Interactions – Its Mechanisms and Methods for Study. FEMS Microbiol. Rev. 1999, 23, 179-230

(5) Karaky, N.; Kirby, A.; McBain, A.; Butler, J.; El Mohtadi, M.; Banks, C.; Whitehead, K. Metal Ions and Graphene-Based Compounds as Alternative Treatment Options for Burn Wounds Infected by Antibiotic-Resistant *Pseudomonas aeruginosa*. Arch. Microbiol. 2020, 1-10

(6) Whitehead, K.; Verran, J. Formation, Architecture and Functionality of Microbial Biofilms in the Food Industry. Curr. Op. Food Sci. 2015, 2, 84-91

(7) Feng, G.; Cheng, Y.; Wang, S.; Borca-Tasciuc, D.; Worobo, R.; Moraru, C. Bacterial Attachment and Biofilm Formation on Surfaces are Reduced by Small-Diameter Nanoscale Pores: How Small is Small Enough?. NPJ Biofilms Microbiomes 2015, 1, 1-9

(8) Percival, S.; Suleman, L.; Vuotto, C.; Donelli, G. Healthcare-Associated Infections, Medical Devices and Biofilms: Risk, Tolerance and Control. J. Med. Microbiol. 2015, 64, 323-334

(9) Mills, M.; Lee, J. The Threat of Carbapenem-Resistant Bacteria in the Environment: Evidence of Widespread Contamination of Reservoirs at a Global Scale. Environ. Poll. 2019, 255, 1131-1143

(10) Doll, M.; Stevens, M.; Bearman, G. Environmental Cleaning and Disinfection of Patient Areas. Inter. J. Infec. Dis. 2018, 67, 52-57

(11) Vatanpour, V.; Shockravi, A.; Zarrabi, H.; Nikjavan, Z.; Javadi, A. Fabrication and Characterization of Anti-Fouling and Anti-Bacterial Ag-Loaded Graphene Oxide/Polyethersulfone Mixed Matrix Membrane. J. Ind. Eng. Chem. 2015, 30, 342-352

(12) Wang, G.; Zhu, L.; Liu, H.; Li, W. Zinc-Graphite Composite Coating for Anti Fouling Application. Mat. Lett. 2011, 65, 3095-3097

(13) Whitehead, K.; Vaidya, M.; Liauw, C.; Brownson, D.; Ramalingam, P.; Kamieniak, J.; Rowley-Neale, S.; Tetlow, L.; Wilson-Nieuwenhuis, J.; Brown, D.; McBain, A.; Kulandaivel, J.; Banks, C. Antimicrobial Activity of Graphene Oxide-Metal Hybrids. Inter. Biodeter. Biodeg. 2017, 123, 182-190

(14) Slate, A.; Wickens, D.; El Mohtadi, M.; Dempsey-Hibbert, N.; West, G.; Banks, C.; Whitehead, K. Antimicrobial Activity of Ti-ZrN/Ag Coatings for use in Biomaterial Applications. Sci. Rep. 2018, 8, 1-12

(15) Ackermann, S.; Steimecke, M.; Morig, C.; Spohn, U.; Bron, M. A Complementary Raman and SECM Study on Electrically Conductive Coatings Based on Graphite Sol-Gel Composite Electrodes for the Electrochemical Antifouling. J. Electroanal. Chem. 2017, 795, 68-74

(16) Kumar, P.; Huo, P.; Zhang, R.; Liu, B. Antibacterial Properties of Graphene-Based Nanomaterials. Nanomat. 2019, 9, 737-769

(17) Shukla, A.; Alam, J.; Ansari, M.; Alhoshan, M.; Ali, F. Antimicrobial and Antifouling Properties of Versatile PPSU/Carboxylated GO Nanocomposite Membrane Against Gram-Positive and Gram-Negative Bacteria and Protein. Environ. Sci. Poll. Res. 2018, 25, 34103-34113

(18) Slate, A. J.; Karaky, N.; Whitehead K. A. Antimicrobial Properties of Modified Graphene and other Advanced 2D Material Coated Surfaces. In: Advanced 2D Material - Characterization, Production and Applications, 2018; 5, 1-19

(19) Xu, M.; Liang, T.; Shi, M.; Chen, H. Graphene-Like Two-Dimensional Materials. Chem. Rev. 2013, 113, 3766-3798

(20) Lembke, D.; Bertolazzi, S.; Kis, A. Single-Layer MoS2 Electronics. Accounts of Chem. Res. 2015, 48, 100-110

(21) Wang, Z.; Mi, B. Environmental Applications of 2D Molybdenum Disulfide (MoS_2) Nanosheets. Environ. Sci. Tech. 2017, 51, 8229-8244

(22) Alam, J.; Shukla, A.; Alhoshan, M.; Arockiasamy Dass, L.; Muthumareeswaran, M.; Khan, A.; Ahmed Ali, F. Graphene Oxide, an Effective Nanoadditive for a Development of Hollow Fiber Nanocomposite Membrane with Antifouling Properties. Adv. Polymer Tech. 2018, 37, 2597-2608

(23) Whitehead, K.; Verran, J. The Effect of Surface Properties and Application Method on the Retention of *Pseudomonas aeruginosa* on Uncoated and Titanium-Coated Stainless Steel. Inter. Biodeter. Biodeg. 2007, 60, 74-80

(24) Wickens, D.; Lynch, S.; West, G.; Kelly, P.; Verran, J.; Whitehead, K. Quantifying the Pattern of Microbial Cell Dispersion, Density and Clustering on Surfaces of Differing Chemistries and Topographies Using Multifractal Analysis. J. Microbiol. Meth. 2014, 104, 101-108

(25) Moreira, J.; Gomes, L.; Whitehead, K.; Lynch, S.; Tetlow, L.; Mergulhão, F. Effect of Surface Conditioning with Cellular Extracts on *Escherichia coli* Adhesion and Initial Biofilm Formation. Food Bioproducts Process 2017, 104, 1-12

(26) Tetlow, L.; Lynch, S.; Whitehead, K. The Effect of Surface Properties on Bacterial Retention: A Study Utilising Stainless Steel and TiN/25.65at.%Ag Substrata. Food Bioproducts Process 2017, 102, 332-339

(27) Sigma Aldritch. 2020. Molybdenum(IV) Sulfide. [online] Available at: <https://www.sigmaaldrich.com/catalog/substance/molybdenumivsulfide160071317335l1?lang=en&region=GB> (Accessed 8 April 2020)

(28) Naves, P.; del Prado, G.; Huelves, L.; Gracia, M.; Ruiz, V.; Blanco, J.; Rodrguez Cerrato, V.; Ponte, M.; Soriano, F. Measurement of Biofilm Formation by Clinical Isolates of *Escherichia coli* is Method-Dependent. J. Appl. Microbiol. 2008, 105, 585-590

(29) Whitehead, K.; Benson, P.; Smith, L.; Verran, J. The Use of Physicochemical Methods to Detect Organic Food Soils on Stainless Steel Surfaces. Biofouling 2009, 25, 749-756

(30) MacCallum, N.; Howell, C.; Kim, P.; Sun, D.; Friedlander, R.; Ranisau, J.; Ahanotu, O.; Lin, J.; Vena, A.; Hatton, B.; Wong, T.; Aizenberg, J. Liquid-Infused Silicone as a Biofouling-Free Medical Material. ACS Biomat. Sci. Eng. 2014, 1, 43-51

(31) Rowley-Neale, S.; Smith, G.; Banks, C. Mass-Producible 2D-MoS2 Impregnated Screen-Printed Electrodes That Demonstrate Efficient Electrocatalysis Toward the Oxygen Reduction Reaction. ACS Appl. Mat. Interfaces 2017, 9, 22539-22548

(32) Whitehead, K.; Verran, J. The Effect of Surface Topography on the Retention of Microorganisms. Food Bioproducts Process. 2006, 84, 253-259

(33) Flint, S.; Hartley, N. A Modified Selective Medium for the Detection of *Pseudomonas* Species that Cause Spoilage of Milk and Dairy Products. Inter. Dairy J. 1996, 6, 223-230

(34) Whitehead, K.; Colligon, J.; Verran, J. Retention of Microbial Cells in Substratum Surface Features of Micrometer and Sub-Micrometer Dimensions. Colloid. Surf. B: Biointerfaces 2005, 41, 129-138

(35) Whitehead, K.; Rogers, D.; Colligon, J.; Wright, C.; Verran, J. Use of the Atomic Force Microscope to Determine the Effect of Substratum Surface Topography on the Ease of Bacterial Removal. Colloid. Surf. B: Biointerfaces 2006, 51, 44-53

(36) Lee, J.; Dak, P.; Lee, Y.; Park, H.; Choi, W.; Alam, M.; Kim, S. Two Dimensional Layered MoS_2 Biosensors Enable Highly Sensitive Detection of Biomolecules. Sci. Rep. 2014, 7352, 1-7

(37) Zhang, S.; Zeng, X.; Tang, Z.; Tan, M. Exploring the Antisticking Properties of Solid Lubricant Thin Films in Transfer Molding. Inter. J. Modern Phys. B 2002, 16, 1080-1085

(38) Gaur, A.; Sahoo, S.; Ahmadi, M.; Dash, S.; Guinel, M.; Katiyar, R. Surface Energy Engineering for Tunable Wettability through Controlled Synthesis of MoS_2. Nano Lett. 2014, 14, 4314-4321

(39) Kozbial, A.; Li, Z.; Sun, J.; Gong, X.; Zhou, F.; Wang, Y.; Xu, H.; Liu, H.; Li, L. Understanding the Intrinsic Water Wettability of Graphite. Carbon 2014, 74, 218-225

(40) Peyravi, M.; Rahimpour, A.; Jahanshahi, M.; Javadi, A.; Shockravi, A. Tailoring the Surface Properties of PES Ultrafiltration Membranes to Reduce the Fouling Resistance using Synthesized Hydrophilic Copolymer. Microporous Mesoporous Mat. 2012, 160, 114-125

(41) Jucker, B.; Harms, H.; Hug, S.; Zehnder, A. Adsorption of Bacterial Surface Polysaccharides on Mineral Oxides is Mediated by Hydrogen Bonds. Colloid. Surf. B: Biointerfaces 1997, 9, 331-343

(42) Jucker, B.; Harms, H.; Zehnder, A. Polymer Interactions Between Five Gram Negative Bacteria and Glass Investigated using LPS Micelles and Vesicles as Model Systems. Colloid. Surf. B: Biointerfaces 1998, 11, 33-45

(43) Chopra, I. The Increasing Use of Silver-Based Products as Antimicrobial Agents: A Useful Development or a Cause for Concern? —Author's Response. J. Antimicrob. Chemo. 2007, 60, 447-448

(44) Asthagiri, D.; Lenhoff, A. Influence of Structural Details in Modelling Electrostatically Driven Protein Adsorption. Langmuir 1997, 13, 6761-6768

(45) Wittemann, A.; Ballauff, M. Interaction of Proteins with Linear Polyelectrolytes and Spherical Polyelectrolyte Brushes in Aqueous Solution. Physical Chemistry Chemical Physics 2006, 8, 5269-5275

(46) Yuwen, L.; Sun, Y.; Tan, G.; Xiu, W.; Zhang, Y.; Weng, L.; Teng, Z.; Wang, L. MoS_2 Polydopamine-Ag Nanosheets with Enhanced Antibacterial Activity for Effective Treatment of *Staphylococcus aureus* Biofilms and Wound Infection. Nanoscale 2018, 10, 16711-16720

(47) Guiney, L.; Wang, X.; Xia, T.; Nel, A.; Hersam, M. Assessing and Mitigating the Hazard Potential of Two-Dimensional Materials. ACS Nano 2018, 12, 6360-6377

(48) Chang, Y.; Yang, S.; Liu, J.; Dong, E.; Wang, Y.; Cao, A.; Liu, Y.; Wang, H. *In Vitro* Toxicity Evaluation of Graphene Oxide on A549 Cells. Tox. Lett. 2011, 20, 201-210

(49) Fan, J.; Li, Y.; Nguyen, H.; Yao, Y.; Rodrigues, D. Toxicity of Exfoliated MoS_2 and Annealed Exfoliated-MoS_2 Towards Planktonic Cells, Biofilms, and Mammalian Cells in the Presence of Electron Donor. Environ. Sci.: Nano 2015, 2, 370-379

(50) Shah, P.; Narayanan, T.; Li, C.; Alwarappan, S. Probing the Biocompatibility of MoS_2 Nanosheets by Cytotoxicity Assay and Electrical Impedance Spectroscopy. Nanotech. 2015, 26, 1-7

(51) Appel, J.; Li, D.; Podlevsky, J.; Debnath, A.; Green, A.; Wang, Q.; Chae, J. Low Cytotoxicity and Genotoxicity of Two-Dimensional MoS_2 and WS2. ACS Biomat. Sci. Eng. 2016, 2, 361-367

(52) Chng, E.; Sofer, Z.; Pumera, M. MoS_2 Exhibits Stronger Toxicity with Increased Exfoliation. Nanoscale 2014, 6, 14412-14418

(53) Chng, E.; Pumera, M. Toxicity of Graphene Related Materials and Transition Metal Dichalcogenides. RSC Adv. 2015. 4, 3074-3080

(54) Zhang, X.; Zhang, Z.; Zhang, S.; Li, D.; Ma, W.; Ma, C.; Wu, F.; Zhao, Q.; Yan, Q.; Xing, B. Size Effect on the Cytotoxicity of Layered Black Phosphorus and Underlying Mechanisms. Small 2017, 13, 1-11

TABLE OF CONTENTS

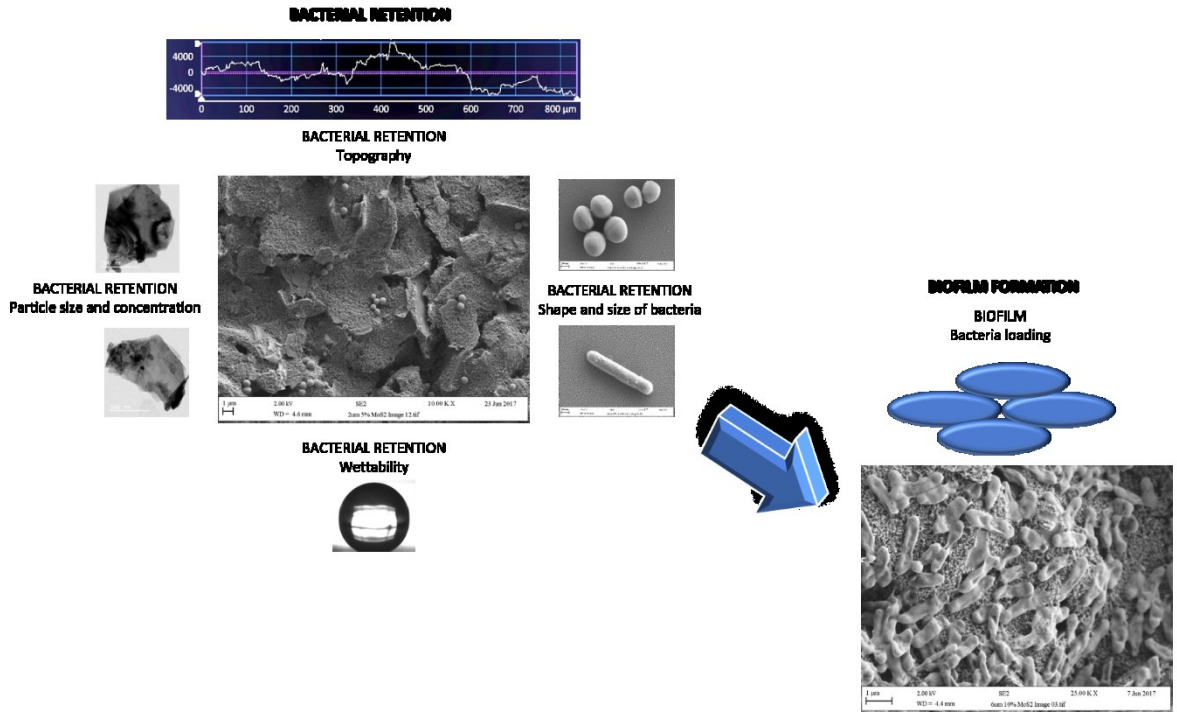

ESI

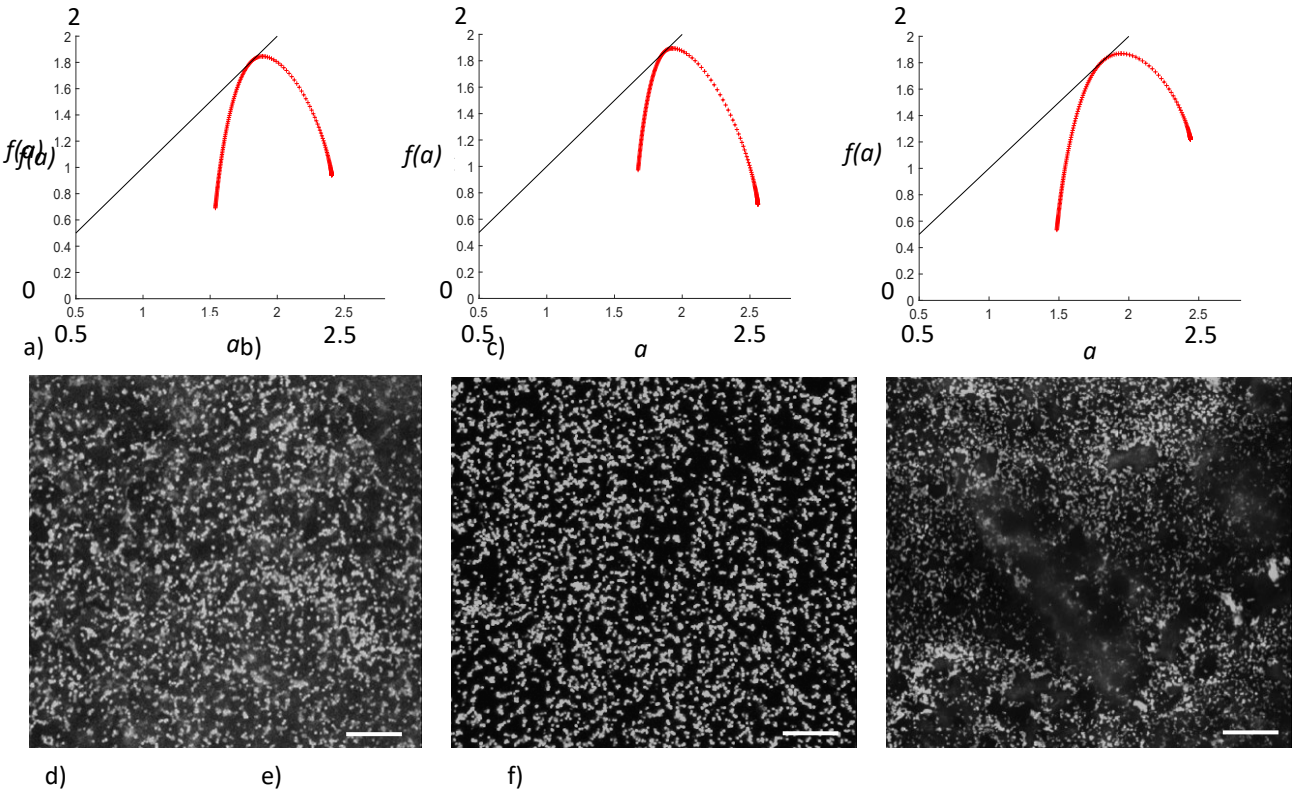

Figure 1. $f(\alpha)$ curves derived for the a) 90 nm, b) 2 µm and c) 6 µm MoS_{2PAR} incorporated into the MoS_{2SUR} derived from the corresponding images following the bacterial retention assays of *P. aeruginosa* on the d) 90 nm, b) 2 µm and c) 6 µm surfaces demonstrating the mathematical information used to determine the percentage coverage, density dispersipon and clustering of *P. aeruginosa.* Error bars are representative of 50 µm.

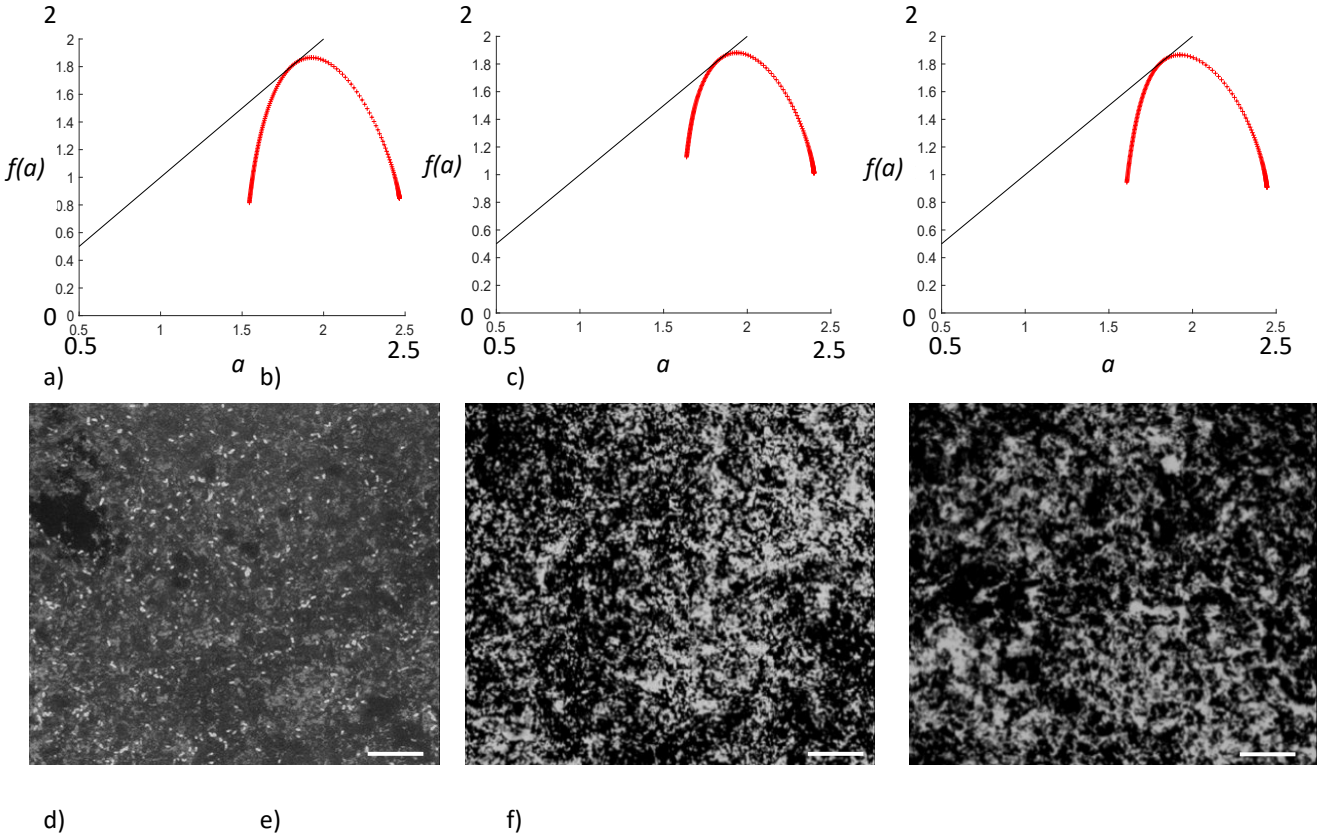

Figure 2. *f* (α) curves derived for the a) 90 nm, b) 2 µm and c) 6 µm MoS_{2PAR} loaded MoS_{2SUR} derived from the corresponding images following the bacterial retention assays of *S. aureus* on the d) 90 nm, b) 2 µm and c) 6 µm surfaces demonstrating the mathematical information used to determine the percentage coverage, density dispersipon and clustering of *S. aureus.* Error bars are representative of 50 µm.